



# Chapter 1.

## VALOR Analysis

looks like a poor choice of title (and, I would guess, structure in this chapter).  
Perhaps separate out a discussion of the general VALOR framework from SBN sensitivity studies using VALOR?

### 1.1. VALOR Framework

The VALencia-Oxford-Rutherford (VALOR) framework is a neutrino fitting framework that was first developed for the Tokai to Kamioka (T2K) experiment, but has since been adapted to also cover Deep Underground Neutrino Experiment (DUNE) and the Short Baseline Neutrino (SBN) program [1]. + also used for HyperK

The data inputs used for an oscillation analysis are mainly provided in the form of Monte Carlo Templates (MCTs), which provide a mapping between true and reconstructed variables. These MCTs,  $T$ , encapsulate a number of quantities describing a given event and are listed below,

- b - Beam configuration
- d - Detector
- s - Sample *Topological event sample or selection?*
- m - Reaction Mode
- r - A bin in reconstructed space *multi-dimensional kinematic*
- t - A bin in true space, *multi-bin kinematic*

May help the reader if you provide some examples of each..

with  $T = T_{d;b;s;m}(r, t)$ . By combining  $T$  with the necessary physics parameters,  $\vec{\theta}$ , and systematic parameters,  $\vec{f}$ , the predicted event rate,  $n_{d;b;s}^{\text{pred}}$ , may be expressed

Starts a bit abruptly and jumps straight into technicalities. Perhaps start a bit more gently, and without equations, explain some of the basics: what is it, what is it meant to be doing, what are the main analysis strategies which are implemented (indirect extrapolation, joint oscillation + systematics fit to kinematic distributions for different topologies from multiple detectors, etc...). What are the advantages of this analysis method?

not well explained: Why the oscillation probability depends on  $m$ ?  
 why does a neutrino cares if it interacts via  $\Delta E$  or  $RES$   
 when it "decides whether to oscillate"? Read how  $P_{d;b;m}$  is applied  
 and the peculiarities with NCs.

$$n_{d;b;s}^{pred}(r; \vec{\theta}; \vec{f}) = \sum_m \sum_t P_{d;b;m}(t; \vec{\theta}) \cdot R_{d;b;s;m}(r, t; \vec{f}) \cdot T_{d;b;s;m}(r, t) \cdot N^{MC}, \quad (1.1)$$

See draft manual on overleaf.

where  $P_{d;b;m}(t; \vec{\theta})$  represents the effect due to a physics hypothesis (e.g. neutrino oscillations),  $R_{d;b;s;m}(r, t; \vec{f})$  represents the response of a MCT bin to the systematic variations and  $N^{MC} = \text{POT}_{b;d}^{\text{data}} / \text{POT}_{b;d}^{MC}$ , which is the normalisation by which to scale the event rate to account for the POT which was used to construct the sample of neutrino events with respect to the nominal POT in the analysis. For  $n_{d;b;s}^{obs}(r)$  observed events, the log likelihood,  $\ln \lambda_{d;b;s}(\vec{\theta}, \vec{f})$ , is given by

$$\ln \lambda_{d;b;s}(\vec{\theta}, \vec{f}) = - \sum_{b,d,s,r} \left\{ \left( n_{d;b;s}^{pred}(r, \vec{\theta}, \vec{f}) - n_{d;b;s}^{obs}(r) \right) + n_{d;b;s}^{obs}(r) \cdot \ln \frac{n_{d;b;s}^{obs}(r)}{n_{d;b;s}^{pred}(r, \vec{\theta}, \vec{f})} \right\}. \quad (1.2)$$

penalize deviation from  
the nominal values of

An additional ~~penalty~~ term is applied to account for the systematic parameters which is defined as,

$$\ln \lambda_{syst}(\vec{f}) = -\frac{1}{2}(\vec{f} - \vec{f}_0)^T \mathbf{V}^{-1} (\vec{f} - \vec{f}_0), \quad (1.3)$$

where  $\vec{f}_0$  is a vector containing the nominal value of all the systematic parameters and  $\mathbf{V}$  is a covariance matrix containing the uncertainties of the systematic parameters [2].

large statistics (many events, not many samples)

In the limit of ~~many samples~~, quantities of the form  $-2\ln \lambda$  have a  $\chi^2$  distribution, hence calculating the log likelihood allows a goodness-of-fit test to be performed [3].

The total goodness-of-fit value is therefore given by,

$$\chi^2_{tot} = -2(\ln \lambda_{d;b;s}(\vec{\theta}, \vec{f}) + \ln \lambda_{syst}(\vec{f})). \quad (1.4)$$

needs explanation!  
why is this an appropriate method for evaluating sensitivities

In order to create confidence regions, fits are performed between a certain *Asimov* dataset and the corresponding MCTs. The Asimov dataset is a dataset where all parameters are set to their nominal values. Two types of confidence regions

does not seem accurate  
MCTs are used to build  $n^{pred}$ .  
Then we fit  $n^{pred}$  to  $n^{data}$ .

check!! Cannot recall off the top of my head.  
But is it not the purpose of  $-\frac{1}{2}$  in the  $\chi^2$  definition so that it is a  $\chi^2$  (without multiplying with the  $-2$ )

(although, perhaps, at some level our fit could be seen as a fit of MCTs)

The difference between the 2 is not very distinct.  
Statistically, they are the same thing and express regions where our model is compatible/incompatible with data.

The main difference is in the input data: no signal vs injected signal may be constructed; an exclusion region and an allowed region. The exclusion region corresponds to the region of parameter space where the null-hypothesis is excluded with a given confidence whereas the allowed region corresponds to the region of parameter space which is allowed for a given confidence for some set of injected oscillation parameters. In the case of exclusion regions, the Asimov dataset corresponds to the case where no oscillation are observed which is the null-hypothesis and for allowed regions, the oscillation parameters are set to that of the injected signal. For the MCTs, the oscillation parameters are set to a given value and the systematic parameters, if any, are allowed to float up to  $\pm 5\sigma$  from their nominal value. The relevant phase space for each of the three analysis channels considered is split into a  $40 \times 40$  grid. This number was chosen in order to find a balance between having a sufficient granularity when constructing contours without having excessive computing times. The dimensions of the phase space considered are different for each analysis channel and are listed in Table 1.1. Once a fit has been performed for each of the  $40 \times 40$  points, a contour of constant  $\chi^2$  is constructed. The  $\chi^2$  value is chosen such that it corresponds to a certain confidence level,  $CL$ , which for SBN analyses is typically  $5\sigma$ . The critical value of  $\chi^2$ ,  $\chi_{critical}^2$ , corresponding to a  $5\sigma$  confidence level along with a number of other  $\chi_{critical}^2$  values with their associated confidence levels which are commonly seen in literature are outlined in Table 1.2. An example of a 2D  $\chi^2$  surface with exclusion contours of different confidence levels for the  $\nu_e$  appearance channel is shown in Figure 1.12.

Not sure about this definition.  
It is a bit circular (exclusion is... the region excluded).

Also, make

sure you understand

the distinction between Analysis Channel

confidence and  
credible intervals.

Confidence intervals is not

about degree of belief,  
but merely about compatibility

be-

Analysis Channel	Phase Space Considered	
	$\sin^2 2\theta$	$\Delta m_{41}^2$
$\nu_\mu$ Disappearance	$\theta_{\mu\mu}$ : $[10^{-3} - 1]$	$[10^{-2} - 10^2]$ eV $^2$
$\nu_e$ Appearance	$\theta_{\mu e}$ : $[10^{-5} - 1]$	$[10^{-2} - 10^2]$ eV $^2$
$\nu_e$ Disappearance	$\theta_{ee}$ : $[10^{-2} - 1]$	$[10^{-2} - 10^2]$ eV $^2$

Table 1.1.: The phase space considered when constructing contours for each of the three oscillation channels within SBN.

Structure is not quite right: Descriptions of the value  
 framework, statistical methodologies, S&N implementation specifics,  
 Validations, basic analysis inputs, various higher level physics

Confidence level	68%	90%	95%	99%	$3\sigma$	$5\sigma$	studies are all mixed
$\chi^2_{critical}$	0.23	1.64	2.71	5.41	7.74	23.66	together

**Table 1.2.:** The  $\chi^2_{critical}$  values corresponding to various confidence levels which are commonly used when performing sensitivity studies. The confidence levels and  $\chi^2_{critical}$  are related via  $CL = \int_0^{\chi^2_{critical}} \frac{e^{-x/2} x^{u/2-1}}{2^{u/2} \Gamma(u/2)} dx$ , where  $u$  is the degrees of freedom (in this case 1) and  $\Gamma$  is the Gamma function [4].

## 1.2. Systemic Uncertainties

Before the flux and interaction systematics contained in the input files can be consumed by VALOR, they first need to be processed. Depending on whether a given systematic parameter is entirely uncorrelated or not, this is done in two different ways. For the uncorrelated parameters, this is done by constructing a set of associated response functions which represent the impact on the event rate that tweaking a given systematics parameter will have. For a given systematic parameter, individual response functions are constructed for each combination of  $d$ ,  $b$ ,  $s$ ,  $m$ ,  $r$  and  $t$ . Each response function is a 13 knot spline which nominally represents the change in event rate from parameter variations ranging from  $[-3, +3]\sigma$  in  $0.5\sigma$  intervals. The response functions are constructed by first identifying the 12 universes which have a variation closest to each of the non-zero  $\sigma$  intervals and then taking the ratio of the event rate from the selected universe in a 2D ( $r$ ,  $t$ ) bin to the nominal events rate in that bin. By definition there will be a knot at  $0\sigma$  with a response of 1, however, in most cases the remaining 12 knots will not be exactly at  $0.5\sigma$  intervals.

For the case of correlated parameters, it is not straightforward to construct response functions as was done for the uncorrelated parameters because any variations will be due to multiple parameters. These parameters are instead represented by a covariance matrix. Matrices of this type,  $C_{ij}$ , are constructed such that,

$$C_{ij} = \frac{1}{U} \sum_{u=1}^U (N_i^u - N_i^{cv})(N_j^u - N_j^{cv}), \quad (1.5)$$

what is  
 the  
 motivation  
 for all  
 of that?  
 Why what  
 is in the  
 files needs  
 processing?

what is in  
 the files?? There is plenty to  
 explain here.

an important section  
 but starting with "what  
 is in the files" is  
 a very  
 superficial  
 take  
 focussing  
 on  
 mechanics

Make it  
 more  
 physics  
 oriented

what you  
 have  
 here is  
 a sub-  
 subsection  
 of the  
 systematic  
 section

where  $U$  is the number of universes,  $N_{i,j}^u$  is the event rate in universe  $u$  in bin  $i$  or  $j$  and  $N_{i,j}^{cv}$  nominal event rate in bin  $i$  or  $j$ .

### 1.2.1. Validating Systematic Uncertainties

In order to establish that the systematic parameters are being correctly handled within VALOR, a comparison between the event rate variations as seen by VALOR and those obtained directly from the universe files is performed. This is done in two different ways;

1. Tweak the nominal spectra using the response functions within VALOR for a single systematic parameter and then compare with the spectra that were obtained directly from the universe files.
2. Generate  $N$  toy samples (typically 500 in order to match the total number of universes) with some set of systematic parameters randomly tweaked. The one sigma spread from all the toys is found. This is done for both VALOR and for the universe files and the results are compared.

As an example, the  $+1\sigma$  variation for the *horncurrent\_FluxUnisim*, *genie\_ccresAxial* and *genie\_ResDecayGamma* parameters from the  $\nu_e$  sample in Short Baseline Near Detector (SBND) between the VALOR response functions and the universes are shown in Figure 1.1<sup>1</sup>. A complete list of the  $+3\sigma$  variation comparisons for all the uncorrelated systematic parameters in SBND are shown for the  $\nu_e$  appearance channel in Appendix B. In all cases there is either perfect agreement or differences of only up to a few tens of events. It should be noted that the event rate shown in the spectra used for validating the systematic parameters for the  $\nu_e$  channel is several orders of magnitude greater than the nominal event rates as seen in for example Figure 1.7. This is due to manually setting the oscillation parameters to  $\sin^2 2\theta_{\mu e} = 1$  and  $\Delta m_{41}^2 = 100$  eV<sup>2</sup> which ensures that many of the events from the oscillated  $\nu_\mu \rightarrow \nu_e$  sub-sample are processed which is required because the response functions are indexed by mode and therefore contributions from all the sub-samples are needed. Since oscillation and systematic

---

<sup>1</sup>The terms *spline* and *response function* are used interchangeably.

Eg *genie\_ccresAxial* could be  $f_{M_A}^{ccres}$

Basically all systematic parameters could be  $f_{\text{Something}}$ .  
A table somewhere upfront could define them all once and for all.

effects commute, this approach is sufficient to correctly produce a complete set of response functions. In the nominal event rate spectra the assumption is that no oscillation occur so no events from the oscillated sample are included hence the much lower event rate.

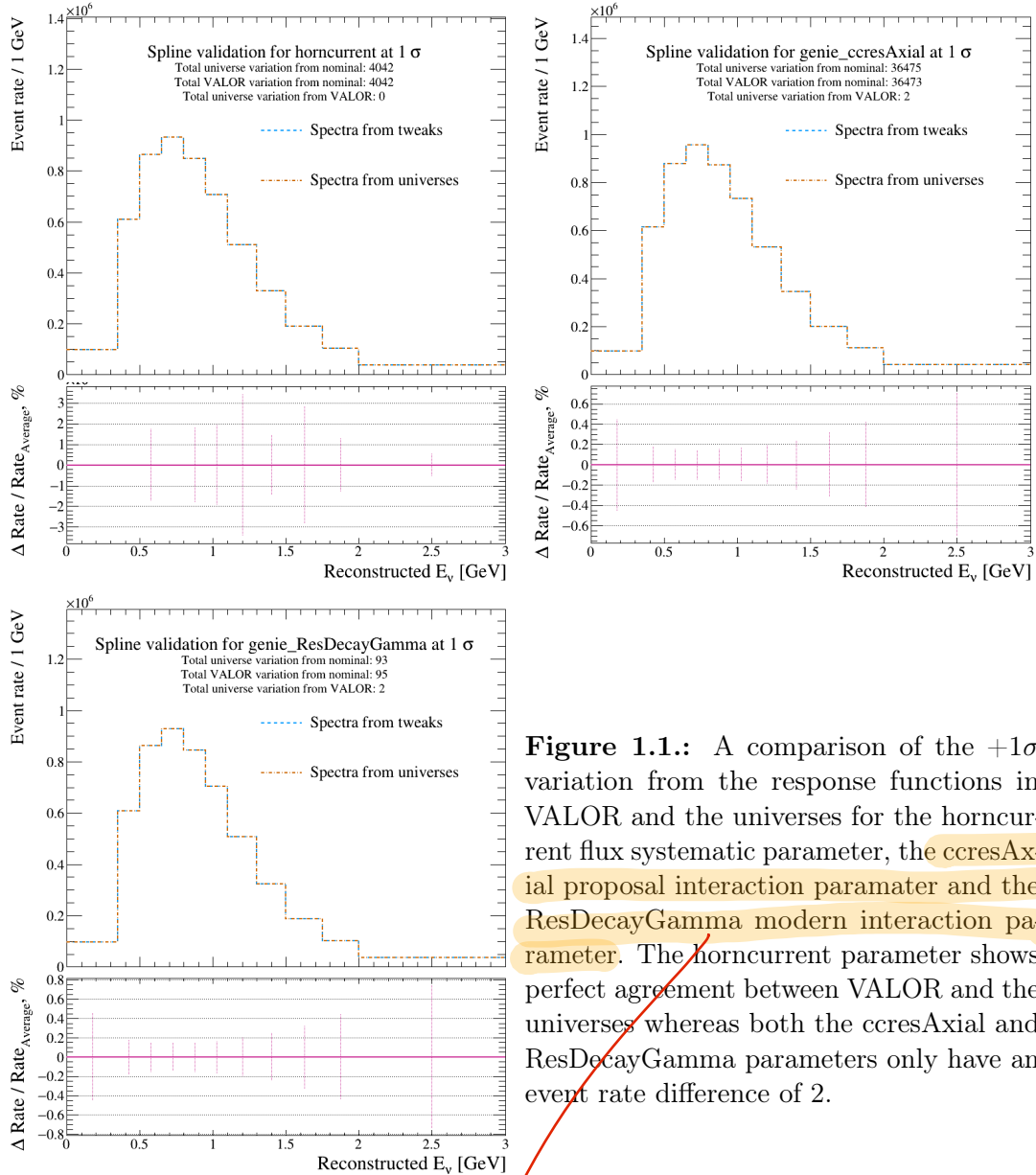


**Figure 1.1.:** A comparison of the  $+1\sigma$  variation from the response functions in VALOR and the universes for the horncurrent flux systematic parameter, the ccresAxial proposal interaction parameter and the ResDecayGamma modern interaction parameter. The horncurrent parameter shows perfect agreement between VALOR and the universes whereas both the ccresAxial and ResDecayGamma parameters only have an event rate difference of 2.

Figure 1.2 shows a double ratio comparison from VALOR and the universes for the flux, proposal interaction and modern interaction systematic parameters. These

needs to be more  
readable - there is  
a lot of internal slang  
here

plots are constructed by first finding the ratio between the  $1\sigma$  variation and the nominal using VALOR and the analogous ratio using the universe files. The double ratio is then constructed by taking the ratio of both the previous  $1\sigma$  ratios. There are some minor differences between the variation in VALOR and the universes, however, even perfect agreement isn't expected since the  $1\sigma$  variations are found by taking the average from many toy samples. Nevertheless, the disagreement is for the most part  $< 1\%$  with a maximum of just over 2%.



are we satisfied with this?

- Do we need any discussion to demonstrate that this is sufficient accuracy?
- Do we need to include any discussion on the reasons of this discrepancy? (do we know?)

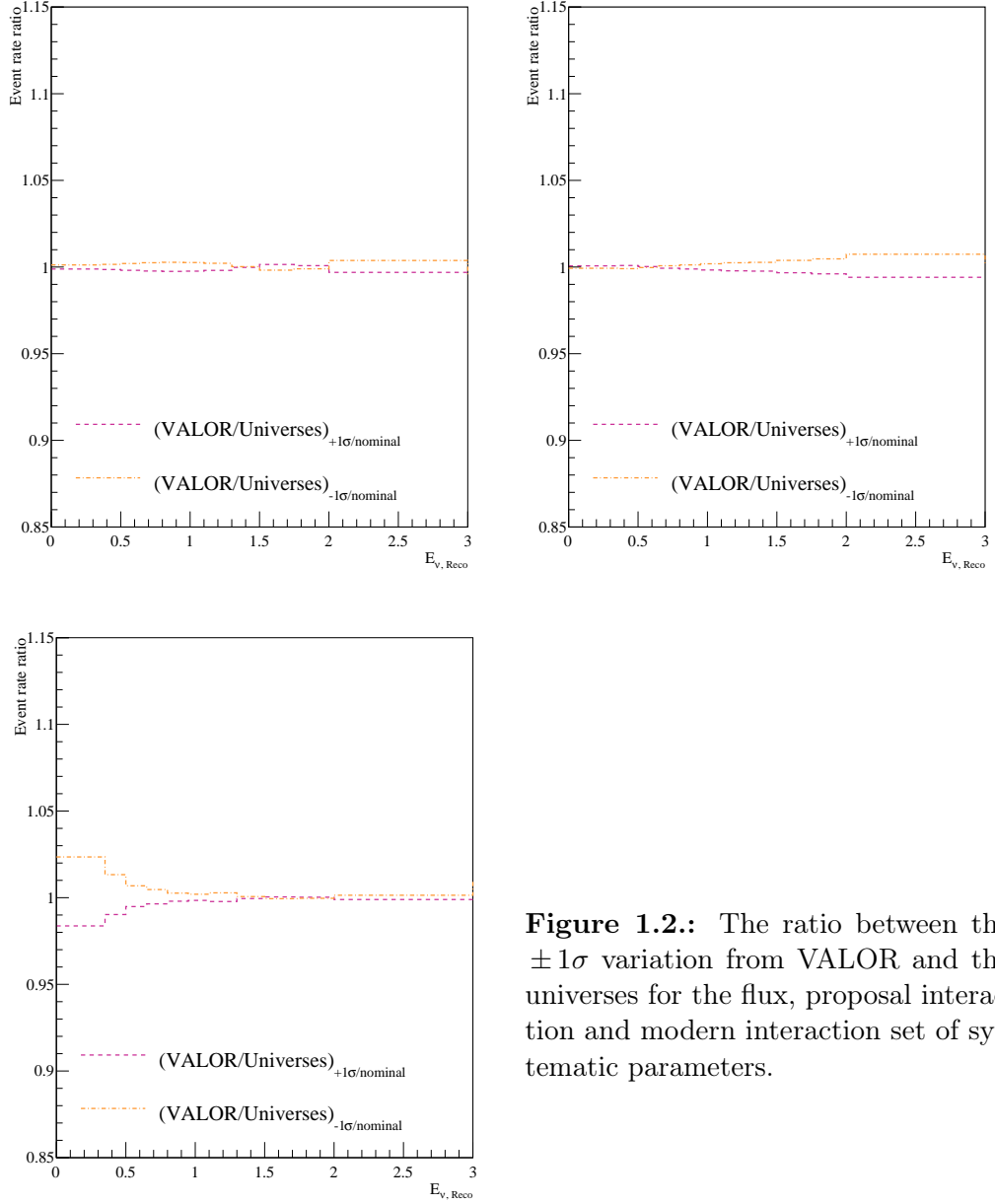


**Figure 1.2.:** The ratio between the  $\pm 1\sigma$  variation from VALOR and the universes for the flux, proposal interaction and modern interaction set of systematic parameters.

depends on the objective / narrative

Could revisit this question in a later draft, when I have a better picture of how everything fits together

**1.2.2. Impact of systematic uncertainties**

Not sure where best to put this section? Here or along with the sensitivity curves?

To assess the impact of the different systematic parameters on the oscillation parameters the following study is performed;

1. Generate a toy experiment with a given oscillation signal with a single systematic parameter,  $f_i$ , set to  $\pm 1\sigma$  from its nominal value and all other systematic parameters are set to their nominal value.
2. Perform a fit on the toy experiment with  $f_i$  fixed to its nominal value. Both the oscillation parameters and all the systematic parameters are initially set to their nominal value and are allowed to float with the exception of  $f_i$ . The other systematic parameters are allowed to float in order to obtain the best possible agreement between the fit and the toy experiment.
3. Steps 1. and 2. are then repeated for all  $i$  systematic parameters of interest. Both the  $+1\sigma$  and  $-1\sigma$  variations should be performed for each systematic parameter since the effect on the oscillation parameters is typically not symmetric.

If  $f_i$  were allowed to float it would be expected that the fit would be able to recover the same oscillation parameters used in the toy experiment since the same Monte Carlo (MC) was used for the toy experiment and the fit. By fixing  $f_i$  to its nominal value in the fit, the fit is forced to make a mistake. This results in the fit remapping the changes in  $f_i$  to the oscillation parameters (and the other systematic parameters).

This study was performed for the  $\nu_e$  appearance and disappearance channels using oscillation parameters  $\sin^2 2\theta_{\mu e} = 0.003$ ,  $\Delta m_{41}^2 = 1.32 \text{ eV}^2$  and  $\sin^2 2\theta_{ee} = 0.4$ ,  $\Delta m_{41}^2 = 3 \text{ eV}^2$  respectively and includes the results from all uncorrelated systematic parameters. The results are shown in Figure 1.3 and Figure 1.4. For both oscillation parameters, the ratio of their value after performing the fit to their nominal value,  $\mathcal{R}$ , are shown after having varied  $f_i$  by  $\pm 1\sigma$ . The ratios shown in

Figure 1.3 and Figure 1.4 are always  $\geq 1$  by construction since  $\mathcal{R}$  is defined as,

$$\mathcal{R} = \begin{cases} \frac{\zeta_{fit}}{\zeta_{nom}}, & \text{if } \zeta_{fit} > \zeta_{nom} \\ \frac{\zeta_{nom}}{\zeta_{fit}}, & \text{if } \zeta_{nom} > \zeta_{fit}, \end{cases} \quad (1.6)$$

where  $\zeta \in \{\sin^2 2\theta, \Delta m_{41}^2\}$  and the subscript *nom* and *fit* refer to the nominal value of the oscillation parameters and the values after performing the fit respectively. The arrows are colour coded such that black corresponds to the case where  $\zeta_{fit} > \zeta_{nom}$  and red corresponds to the case where  $\zeta_{nom} > \zeta_{fit}$ .

The impact of the ccresVector, ccresAxial, IntraNukeNcex and pioninexsec parameter on the  $\nu_e$  appearance exclusion sensitivities are shown in Figure 1.5. The parameters were applied one at a time and chosen as some that showed the largest variations in Figure 1.3, ensuring at least one parameter from each systematic subgroup. Similarly, the ccresVector, ccresAxial, IntraNukePIcex and expskin parameters were used for the  $\nu_e$  disappearance channel and the results are shown in Figure 1.6.

is this conclusion relevant to anything else we discuss here?  
Is it possible to create connections in the text?

Does this make sense / do we understand why?

make more readable  
use math symbols for all systematic params (not softw. variables)  
defined in a table somewhere early in the text

Since you have identified some of the dominant systematics,<sup>10</sup> you need to understand where the corresponding uncertainty is coming from + how these systematics are modelled  $\Rightarrow$  likely examiner questions

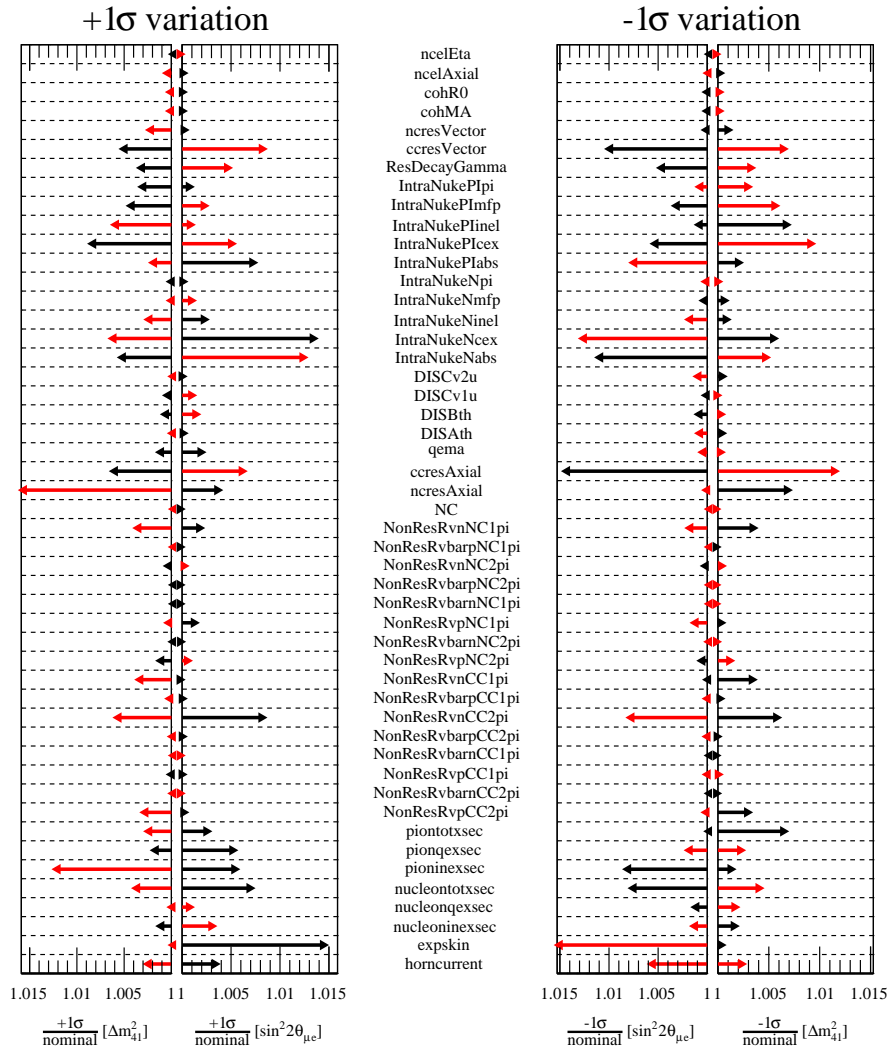


**Figure 1.3.:** The variation in the  $\nu_e$  appearance oscillation parameters due to varying a single systematic parameter at a time by  $\pm 1\sigma$ .

*nice plots*

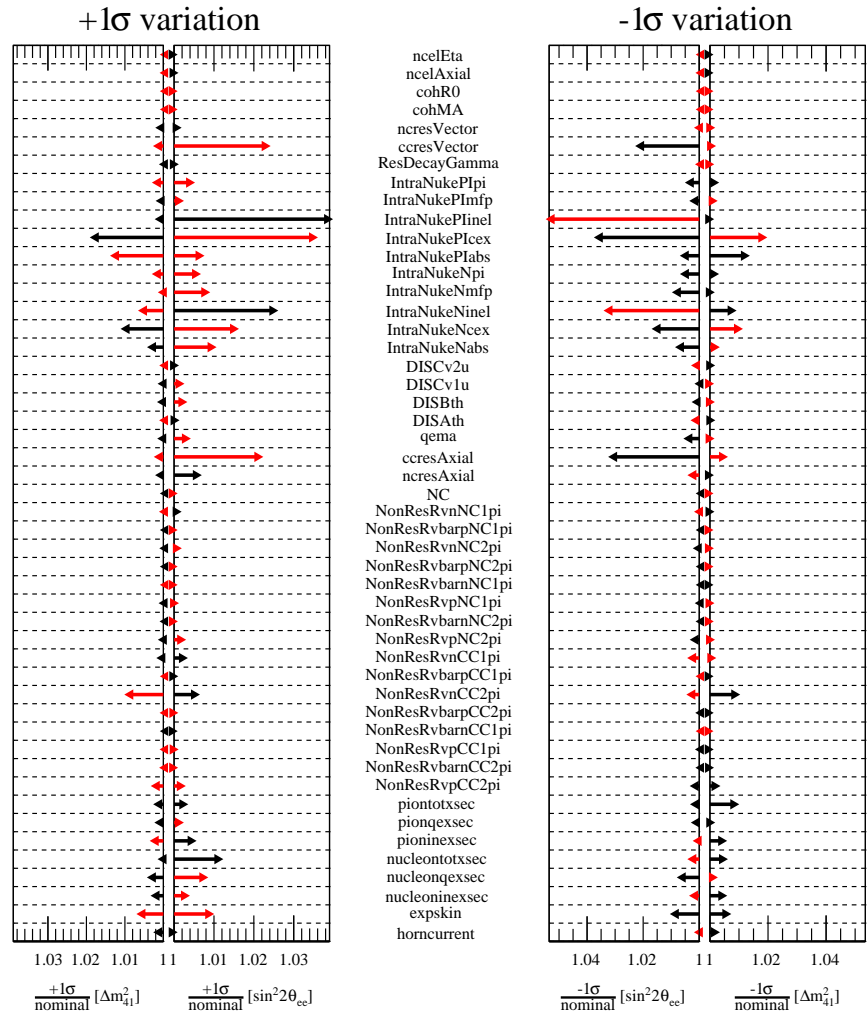


**Figure 1.4.:** The variation in the  $\nu_e$  disappearance oscillation parameters due to varying a single systematic parameter at a time by  $\pm 1\sigma$ .

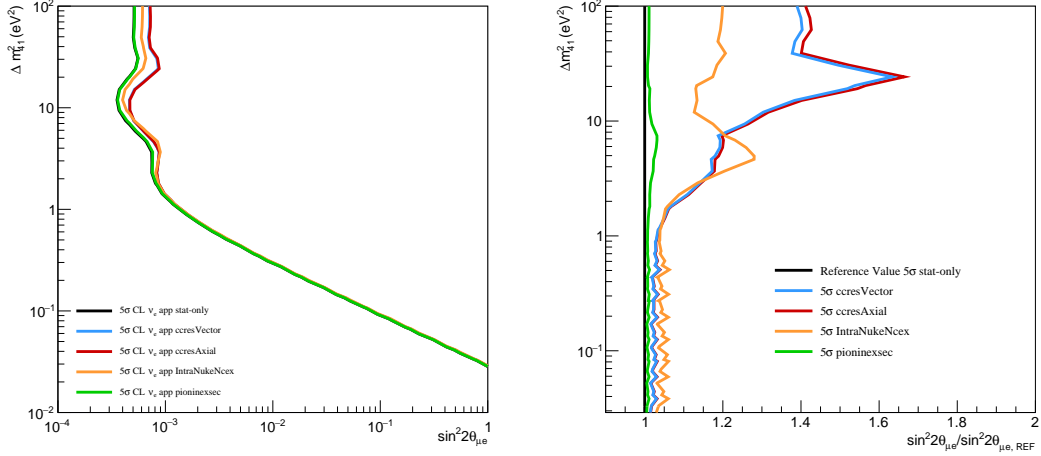


**Figure 1.5.:** Left:  $\nu_e$  appearance exclusion contours with inclusion of a single systematic parameter at a time. The systematic parameters considered are ccresVector, ccresAxial, IntraNukeNcex and pioninexsec. Right: The ratio of the exclusion contours with the inclusion of a systematic parameter the statistical only contour.

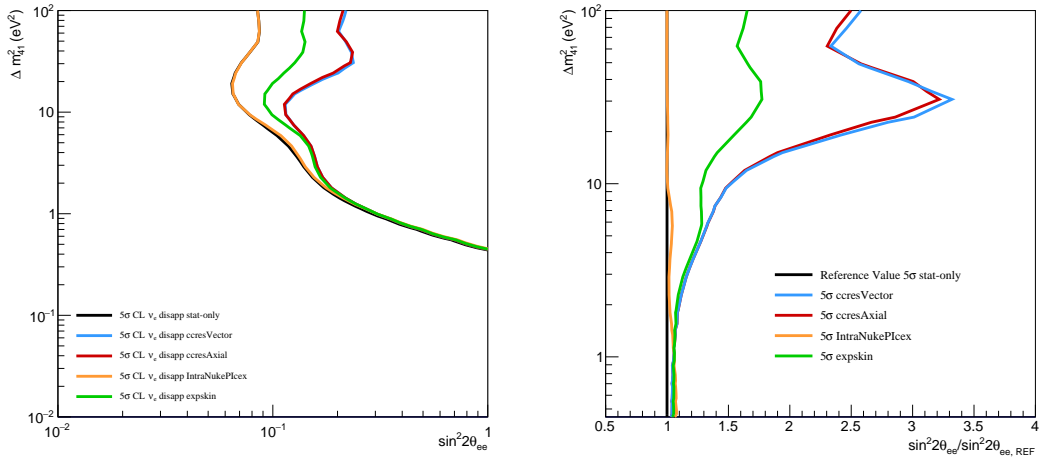


**Figure 1.6.:** Left:  $\nu_e$  disappearance exclusion contours with inclusion of a single systematic parameter at a time. The systematic parameters considered are ccresVector, ccresAxial, IntraNukeNcex and pioninexsec. Right: The ratio of the exclusion contours with the inclusion of a systematic parameter the statistical only contour.

a very technical / functional take on  
the difference / similarities between these 2  
channels. Is there another broader info  
Somewhere else??

### 1.3. $\nu_e$ Analysis

As was mentioned in Section ??, there are two oscillations channels associated with  $\nu_e$ ;  $\nu_e$  appearance and  $\nu_e$  disappearance. Since the only difference between these channels is due to oscillations, the nominal event rates are common between the two.

The breakdown of the nominal number of events by interaction mode and channel is shown numerically in Table 1.3, Table 1.4 and Table 1.5 for SBND, Micro Booster Neutrino Experiment (MicroBooNE) and Imaging Cosmic and Rare Underground Signals (ICARUS) respectively. The same events rates are also shown in Figure 1.7 in the form of spectra. The spectra show the modal breakdown in terms of the coarse reaction modes where the events have been binned in reconstructed neutrino energy.

Similar to Figure 1.7, Figure 1.8 again shows the nominal event rate in each SBN detector, but in an integrated form. Additionally,  $1\sigma$  prefit uncertainty envelopes are shown which are due to the flux and interaction systematics. The accuracy of say the ICARUS prediction can be improved by constraining the systematics from an SBND fit. This is shown in Figure 1.9 which shows the nominal integrated ICARUS spectrum along with the prefit uncertainty envelope as in Figure 1.8, but also a postfit uncertainty envelope based on an SBND fit is shown. The reduction in size from the prefit to postfit envelope highlights the impact of SBND on the ICARUS prediction.

doubt this is  
the first occurrence.

Was they not defined  
earlier? If yes,

just write ICARUS

and MicroBooNE

could become a bit more readable, e.g.

$CC1pi01piC \rightarrow CC1\pi^0\pi^+$  etc

	$\nu_\mu \rightarrow \nu_\mu$	$\bar{\nu}_\mu \rightarrow \bar{\nu}_\mu$	$\nu_e \rightarrow \nu_e$	$\bar{\nu}_e \rightarrow \bar{\nu}_e$	$\nu_\mu \rightarrow \nu_e$	$\bar{\nu}_\mu \rightarrow \bar{\nu}_e$	Non-neutrino	Total
CCQE	17.042	0.000	5957.806	166.618	0.000	0.000	N/A	6141.467
CCMEC	1.149	0.000	1432.965	59.724	0.000	0.000	N/A	1493.837
CC1piC	234.568	0.000	2859.852	112.421	0.000	0.000	N/A	3206.841
CC1pi0	230.739	0.000	513.830	14.641	0.000	0.000	N/A	759.209
CC2piC	19.340	0.000	293.304	7.915	0.000	0.000	N/A	320.559
CC2pi0	5.170	0.000	24.094	0.640	0.000	0.000	N/A	29.904
CC1pi01piC	37.148	0.000	187.022	6.956	0.000	0.000	N/A	231.125
CCcoherent	0.000	0.000	38.137	3.758	0.000	0.000	N/A	41.894
CCnuEEl	0.000	0.000	N/A	N/A	N/A	N/A	N/A	0.000
CCother	20.680	0.000	270.868	8.315	0.000	0.000	N/A	299.863
NCEL	3.447	0.000	0.034	0.000	N/A	N/A	N/A	3.480
NCMEC	0.574	0.000	0.005	0.000	N/A	N/A	N/A	0.579
NC1piC	135.571	0.000	0.839	0.034	N/A	N/A	N/A	136.444
NC1pi0	772.639	0.000	5.539	0.211	N/A	N/A	N/A	778.389
NC2piC	2.298	0.000	0.142	0.000	N/A	N/A	N/A	2.440
NC2pi0	6.893	0.000	0.114	0.005	N/A	N/A	N/A	7.012
NC1pi01piC	16.085	0.000	0.409	0.024	N/A	N/A	N/A	16.518
NCcoherent	76.785	0.000	0.384	0.062	N/A	N/A	N/A	77.231
NC1Gamma	0.000	0.000	0.000	0.000	N/A	N/A	N/A	0.000
NCnuEEl	181.910	0.000	N/A	N/A	N/A	N/A	N/A	181.910
NCother	49.977	0.000	0.520	0.010	N/A	N/A	N/A	50.507
nuEEl	N/A	N/A	0.000	0.000	0.000	0.000	N/A	0.000
cosmic	N/A	N/A	N/A	N/A	N/A	N/A	0.315	0.315
dirt	N/A	N/A	N/A	N/A	N/A	N/A	33.926	33.926
Total	1812.015	0.000	11585.864	381.332	0.000	0.000	34.241	13813.452

Table 1.3.: Nominal  $\nu_e$  event rate breakdown in SBND.

*see before*

	$\nu_\mu \rightarrow \nu_\mu$	$\bar{\nu}_\mu \rightarrow \bar{\nu}_\mu$	$\nu_e \rightarrow \nu_e$	$\bar{\nu}_e \rightarrow \bar{\nu}_e$	$\nu_\mu \rightarrow \nu_e$	$\bar{\nu}_\mu \rightarrow \bar{\nu}_e$	Non-neutrino	Total
CCQE	4.222	0.000	384.923	10.384	0.000	0.000	N/A	399.529
CCMEC	0.056	0.000	93.873	3.658	0.000	0.000	N/A	97.586
CC1piC	18.857	0.000	196.808	7.537	0.000	0.000	N/A	223.202
CC1pi0	19.062	1.041	35.502	1.133	0.000	0.000	N/A	56.739
CC2piC	1.004	0.000	21.942	0.566	0.000	0.000	N/A	23.513
CC2pi0	3.292	0.000	1.882	0.057	0.000	0.000	N/A	5.230
CC1pi01piC	7.160	0.000	13.600	0.606	0.000	0.000	N/A	21.366
CCcoherent	0.000	0.000	2.650	0.374	0.000	0.000	N/A	3.023
CCnueEl	0.000	0.000	N/A	N/A	N/A	N/A	N/A	0.000
CCother	3.310	0.000	19.133	0.442	0.000	0.000	N/A	22.885
NCEL	0.335	0.000	0.003	0.000	N/A	N/A	N/A	0.337
NCMEC	0.000	0.000	0.000	0.000	N/A	N/A	N/A	0.000
NC1piC	13.911	0.000	0.066	0.002	N/A	N/A	N/A	13.979
NC1pi0	59.306	1.004	0.384	0.015	N/A	N/A	N/A	60.710
NC2piC	0.669	0.000	0.007	0.000	N/A	N/A	N/A	0.677
NC2pi0	0.669	0.056	0.009	0.000	N/A	N/A	N/A	0.734
NC1pi01piC	2.269	0.000	0.020	0.001	N/A	N/A	N/A	2.290
NCcoherent	5.505	0.223	0.033	0.003	N/A	N/A	N/A	5.764
NC1Gamma	0.000	0.000	0.000	0.000	N/A	N/A	N/A	0.000
NCnueEl	14.878	0.000	N/A	N/A	N/A	N/A	N/A	14.878
CCother	3.292	0.000	0.049	0.001	N/A	N/A	N/A	3.342
nuEEl	N/A	N/A	0.000	0.000	0.000	0.000	N/A	0.000
cosmic	N/A	N/A	N/A	N/A	N/A	N/A	0.000	0.000
dirt	N/A	N/A	N/A	N/A	N/A	N/A	14.780	14.780
Total	157.796	2.325	770.886	24.778	0.000	0.000	14.780	970.564

**Table 1.4.:** Nominal  $\nu_e$  event rate breakdown in MicroBooNE.

see later

	$\nu_\mu \rightarrow \nu_\mu$	$\bar{\nu}_\mu \rightarrow \bar{\nu}_\mu$	$\nu_e \rightarrow \nu_e$	$\bar{\nu}_e \rightarrow \bar{\nu}_e$	$\nu_\mu \rightarrow \nu_e$	$\bar{\nu}_\mu \rightarrow \bar{\nu}_e$	Non-neutrino	Total
CCQE	4.642	0.000	727.942	19.303	0.000	0.000	N/A	751.887
CCMEC	0.214	0.000	176.496	7.062	0.000	0.000	N/A	183.773
CC1piC	37.383	0.214	372.300	12.894	0.000	0.000	N/A	422.790
CC1pi0	25.814	0.107	64.840	2.157	0.000	0.000	N/A	92.919
CC2piC	4.856	0.107	39.379	1.019	0.000	0.000	N/A	45.361
CC2pi0	2.856	0.107	3.558	0.071	0.000	0.000	N/A	6.592
CC1pi01piC	7.534	0.000	25.844	1.080	0.000	0.000	N/A	34.458
CCcoherent	0.000	0.000	4.953	0.462	0.000	0.000	N/A	5.415
CCnuEEL	0.000	0.000	N/A	N/A	N/A	N/A	N/A	0.000
CCother	2.785	0.000	36.924	0.818	0.000	0.000	N/A	40.526
NCEL	0.536	0.000	0.005	0.000	N/A	N/A	N/A	0.541
NCMEC	0.000	0.000	0.000	0.000	N/A	N/A	N/A	0.000
NC1piC	17.709	0.214	0.130	0.006	N/A	N/A	N/A	18.059
NC1pi0	108.506	0.750	0.705	0.023	N/A	N/A	N/A	109.984
NC2piC	0.750	0.000	0.006	0.000	N/A	N/A	N/A	0.756
NC2pi0	0.857	0.000	0.013	0.000	N/A	N/A	N/A	0.870
NC1pi01piC	3.428	0.107	0.056	0.001	N/A	N/A	N/A	3.592
NCcoherent	11.318	0.428	0.057	0.006	N/A	N/A	N/A	11.810
NC1Gamma	0.000	0.000	0.000	0.000	N/A	N/A	N/A	0.000
NCnuEEL	17.852	0.000	N/A	N/A	N/A	N/A	N/A	17.852
NCother	7.998	0.000	0.079	0.003	N/A	N/A	N/A	8.080
nuEEL	N/A	N/A	0.000	0.000	0.000	0.000	N/A	0.000
cosmic	N/A	N/A	N/A	N/A	N/A	N/A	2.253	2.253
dirt	N/A	N/A	N/A	N/A	N/A	N/A	24.120	24.120
Total	255.037	2.035	1453.287	44.905	0.000	0.000	26.373	1781.637

**Table 1.5.:** Nominal  $\nu_e$  event rate breakdown in ICARUS.

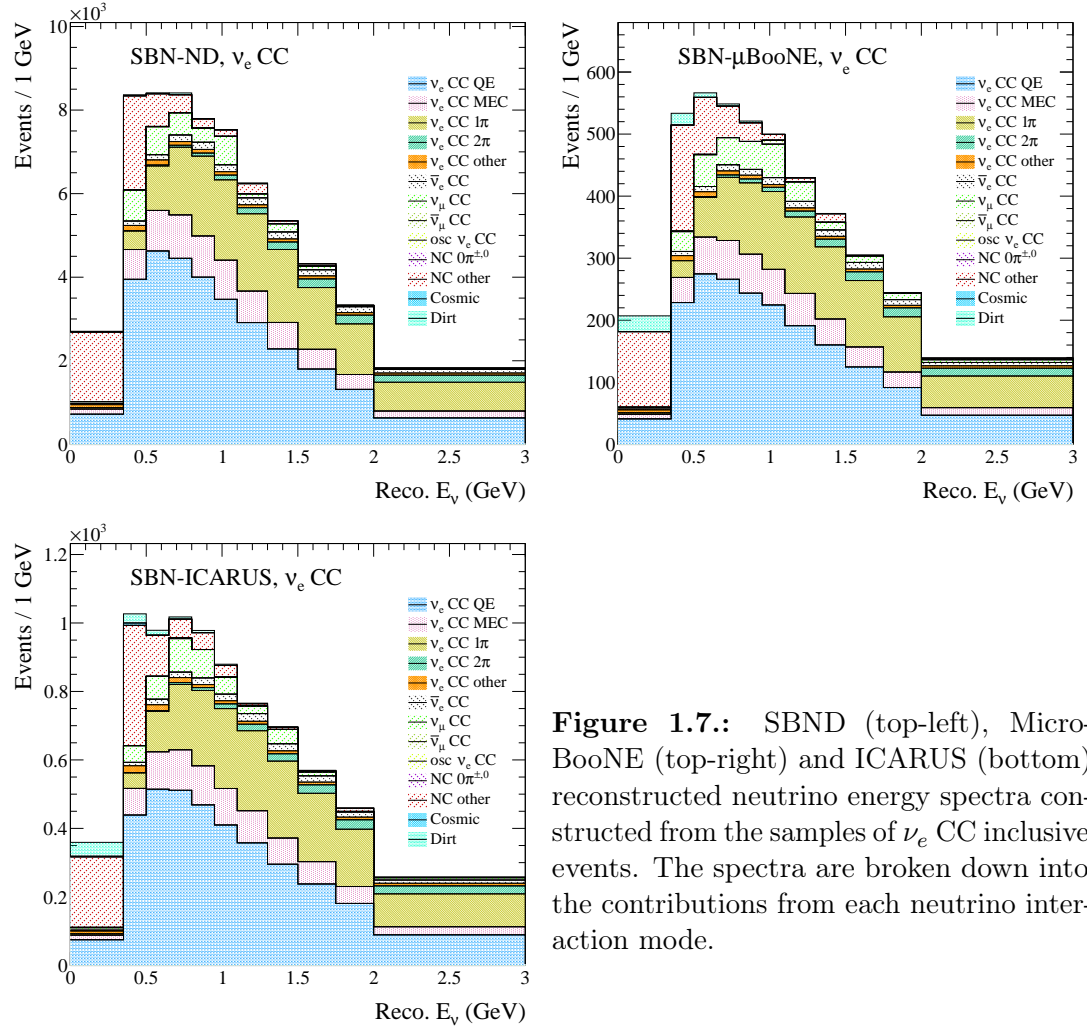


**Figure 1.7.:** SBND (top-left), Micro-BooNE (top-right) and ICARUS (bottom) reconstructed neutrino energy spectra constructed from the samples of  $\nu_e$  CC inclusive events. The spectra are broken down into the contributions from each neutrino interaction mode.

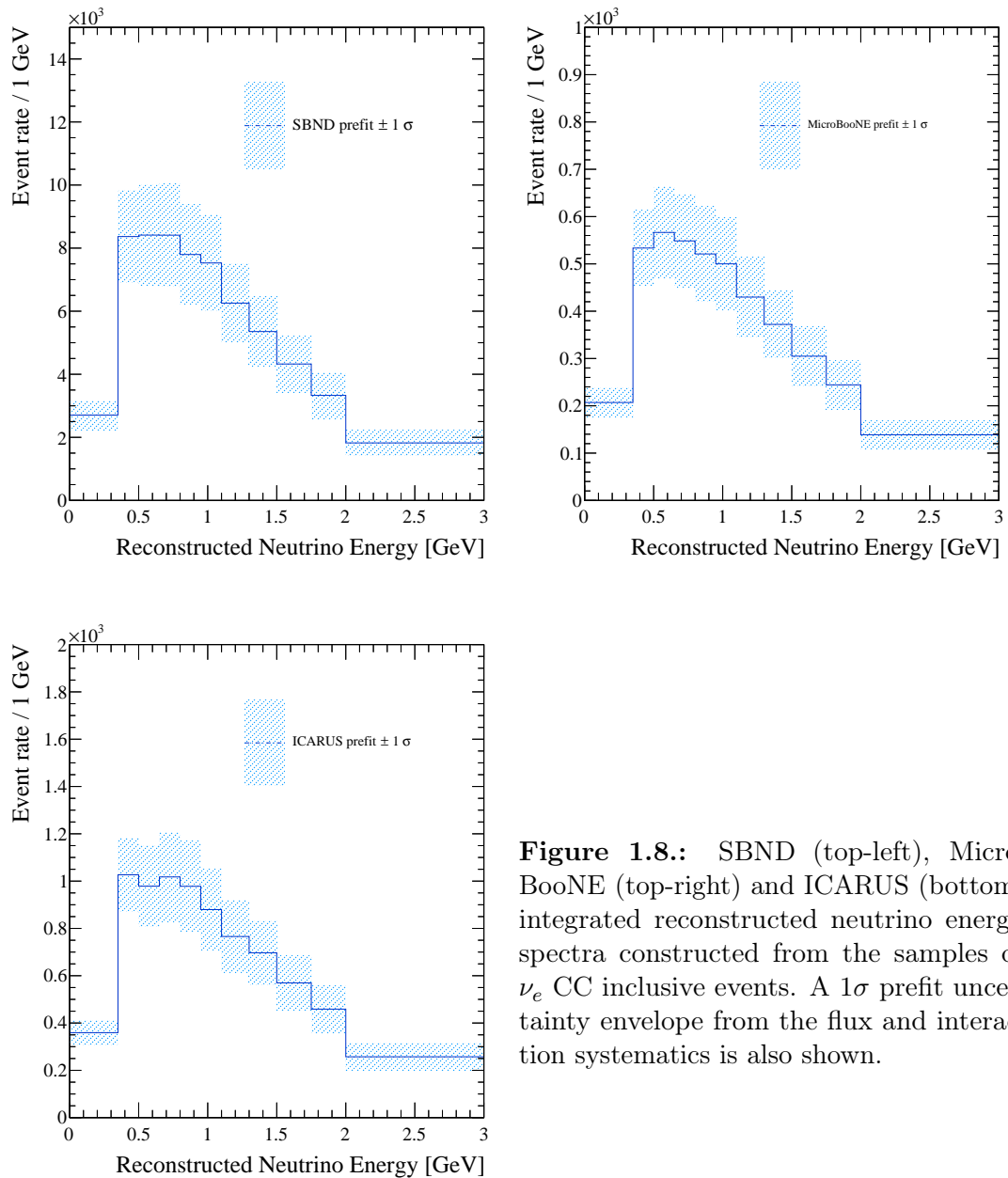


**Figure 1.8.:** SBND (top-left), MicroBooNE (top-right) and ICARUS (bottom) integrated reconstructed neutrino energy spectra constructed from the samples of  $\nu_e$  CC inclusive events. A  $1\sigma$  prefit uncertainty envelope from the flux and interaction systematics is also shown.

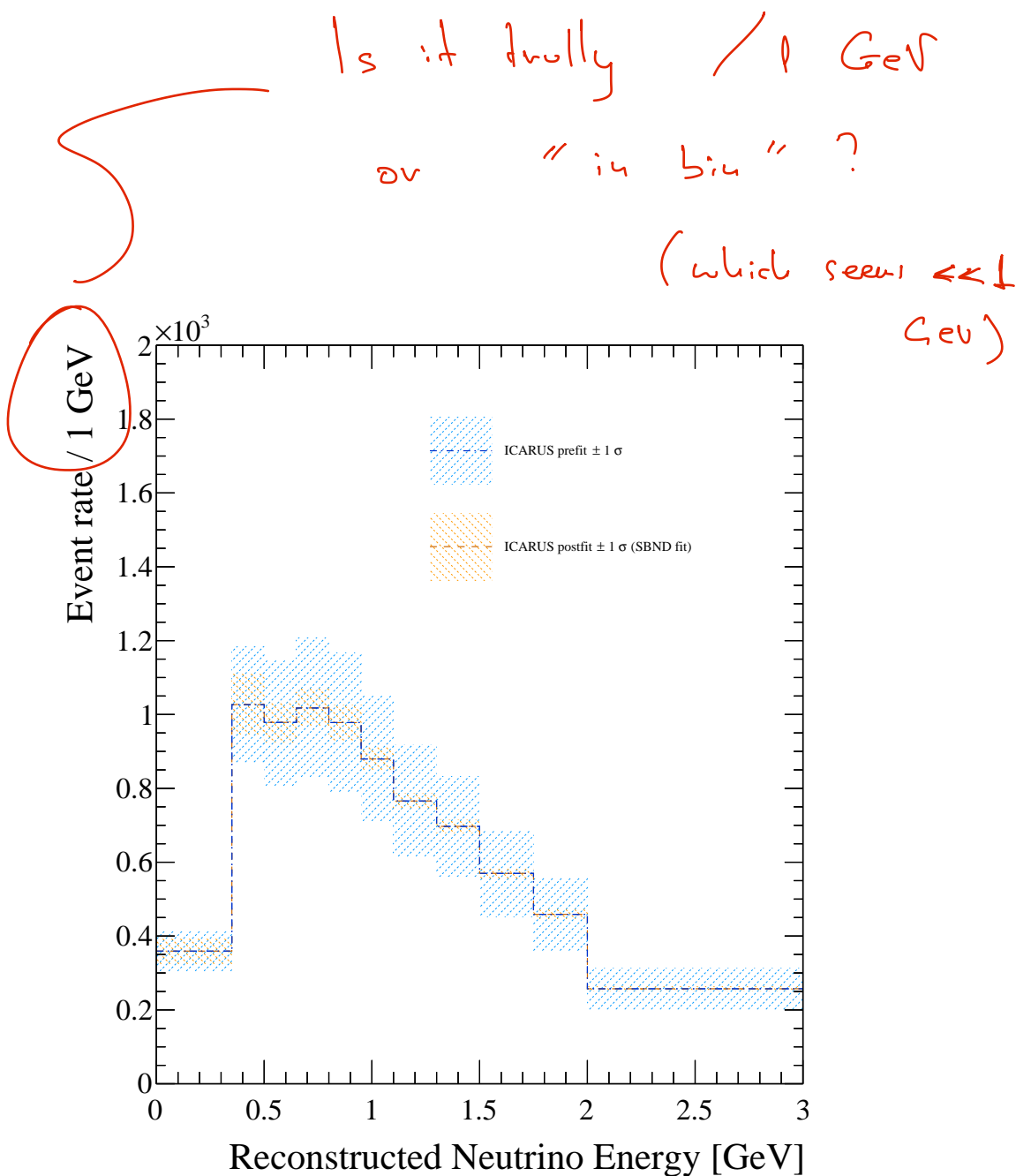


**Figure 1.9.:** ICARUS integrated reconstructed neutrino energy spectrum constructed from the samples of  $\nu_e$  CC inclusive events. The  $1\sigma$  prefit envelope is shown as well as a  $1\sigma$  postfit envelope based on a SBND fit. The reduction in size of the error envelope when going from prefit to postfit shows the impact of SBND on improving the accuracy of the ICARUS prediction.

Perhaps need a slightly different structure  
 here, separating : 20

- motivation for each channel, external limits
- basic understanding each channel in SBND (event rates, impact of systematics, size of expected signal)
- sensitivities

- further studies on sensitivity (e.g. impact of systematics, impact of different detectors etc)

### 1.3.1. $\nu_e$ Appearance Analysis

The  $\nu_e$  appearance channel is concerned with oscillations from  $\nu_\mu$  to  $\nu_e$  and since the oscillation channels are currently considered as stand-alone analyses, an increase in the event rate is expected. This is shown in Figure 1.10 where the nominal event rate breakdown is shown as in Figure 1.7, but overlayed with an integrated spectrum that was produced with oscillation parameters  $\sin^2 2\theta_{\mu e} = 0.003$  and  $\Delta m_{41}^2 = 1.32 \text{ eV}^2$ . The oscillation signal seen for these parameters in SBND is small whereas for MicroBooNE and ICARUS it is substantial which is consistent with what is seen in Figure ???. This highlights the fact that SBND will largely be used to constrain parameters due to observing no or very few oscillated events with the oscillation signal being largely left to MicroBooNE and ICARUS.

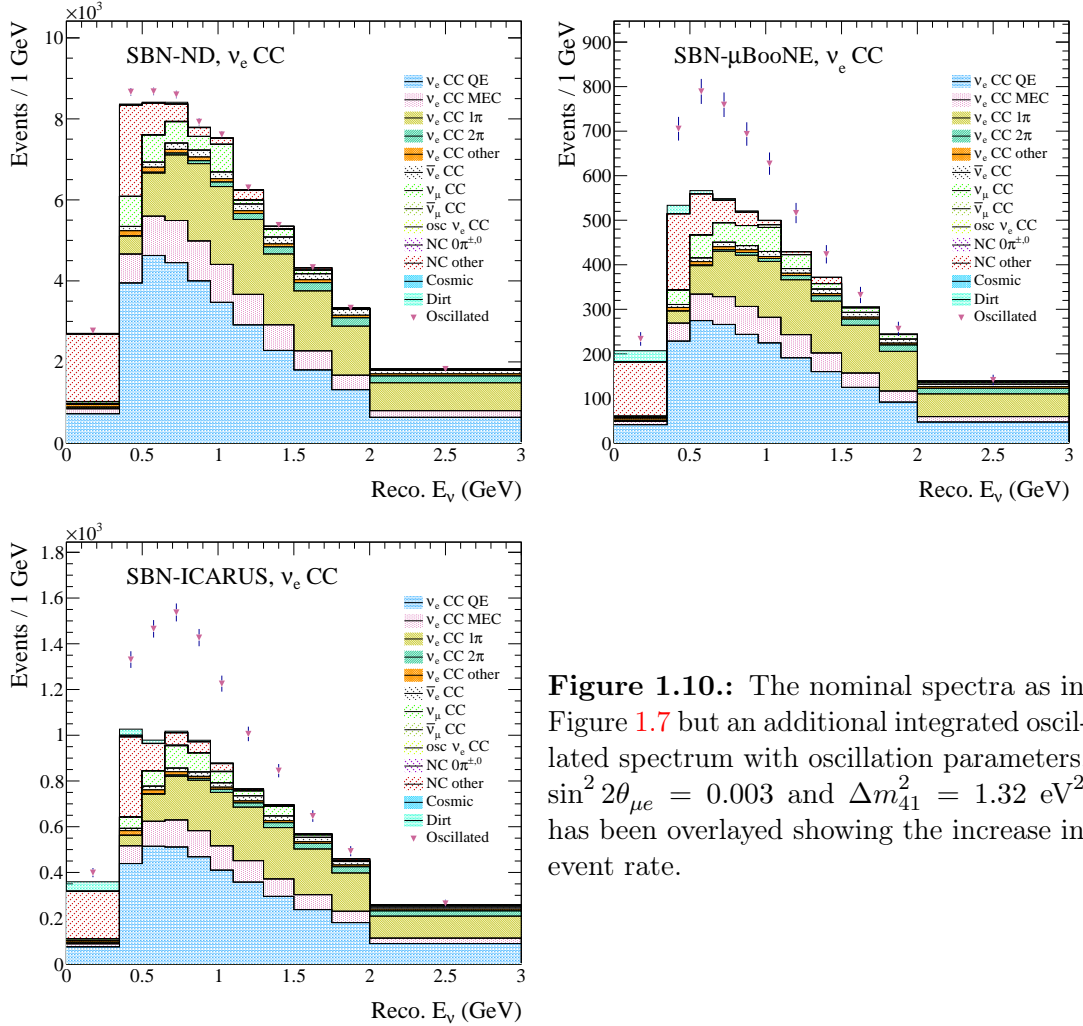


**Figure 1.10.:** The nominal spectra as in Figure 1.7 but an additional integrated oscillated spectrum with oscillation parameters,  $\sin^2 2\theta_{\mu e} = 0.003$  and  $\Delta m_{41}^2 = 1.32 \text{ eV}^2$  has been overlayed showing the increase in event rate.

The top left plot of Figure 1.11 shows the  $\nu_e$  appearance stat only exclusion contour and allowed region from fits combining all three SBN detectors. The injected point  $\Delta m_{41}^2 = 1.32 \text{ eV}^2$ ,  $\sin^2 2\theta_{\mu e} = 0.003$ , used when producing the allowed region is shown along with two further points on the exclusion contour at  $\Delta m_{41}^2 = 1 \text{ eV}^2$ ,  $\sin^2 2\theta_{\mu e} = 0.0014$  and  $\Delta m_{41}^2 = 100 \text{ eV}^2$ ,  $\sin^2 2\theta_{\mu e} = 0.0005$ .  $\nu_e$  appearance spectra are produced using oscillation parameters corresponding to each of these three points for each of the three SBN detectors. The ratio of each of these oscillated spectra to the nominal for each detector are shown in the remaining plots in Figure 1.11 and highlight the expected oscillation signal.

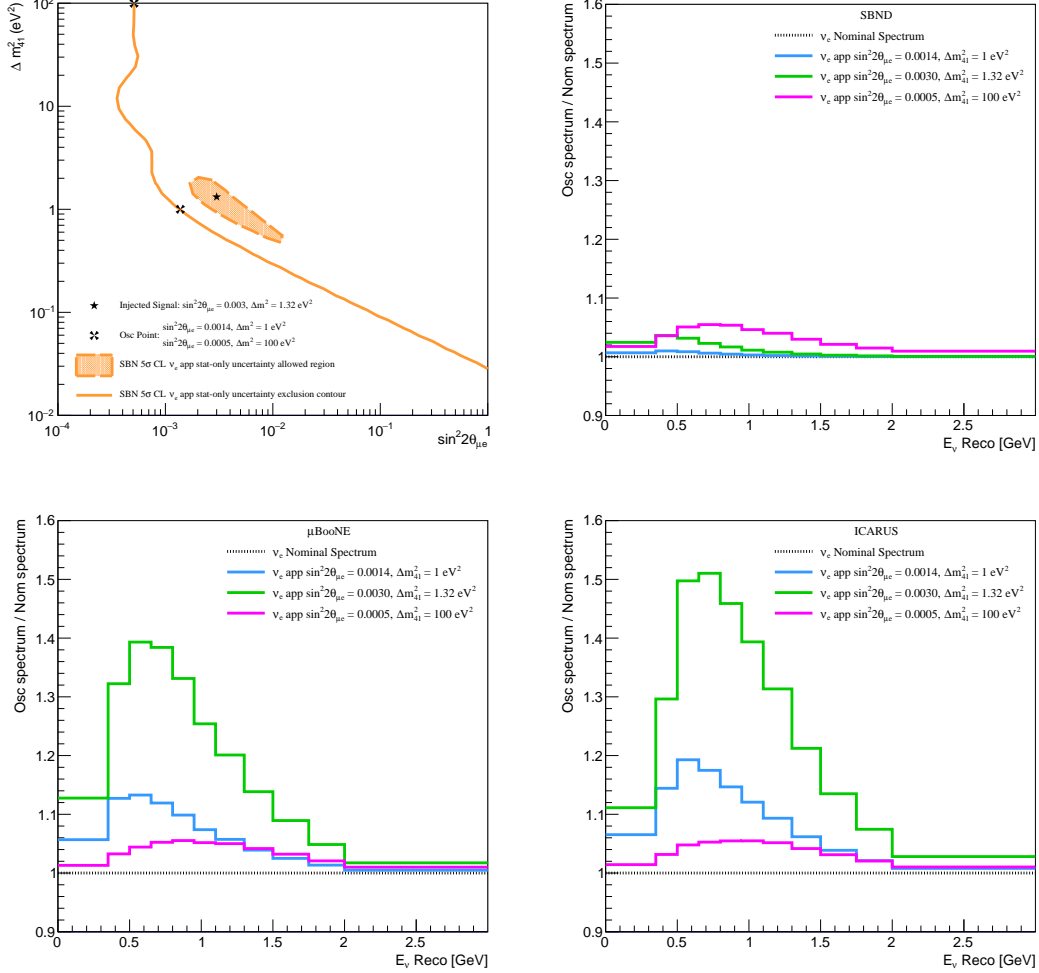


**Figure 1.11.:**  $\nu_e$  appearance stat-only exclusion contour and allowed region. The injected point at  $\sin^2 2\theta_{\mu e} = 0.003$ ,  $\Delta m_{41}^2 = 1.32 \text{ eV}^2$  used for the allowed region is shown along with two further points at  $\sin^2 2\theta_{\mu e} = 0.0014$ ,  $\Delta m_{41}^2 = 1 \text{ eV}^2$  and  $\sin^2 2\theta_{\mu e} = 0.0005$ ,  $\Delta m_{41}^2 = 100 \text{ eV}^2$  (top left). The ratio of spectra with oscillation parameters corresponding to the three points mentioned versus nominal are shown for sbnd (top right), MicroBooNE (bottom left) and ICARUS (bottom right).

An example of the  $\chi^2$  surface as described in Section 1.1 is shown in Figure 1.12 along with contours of constant  $\chi^2$  corresponding to 90%,  $3\sigma$  and  $5\sigma$  confidence levels. The contours have been produced for the entire SBN program with the inclusion of statistical plus flux and interaction systematics.

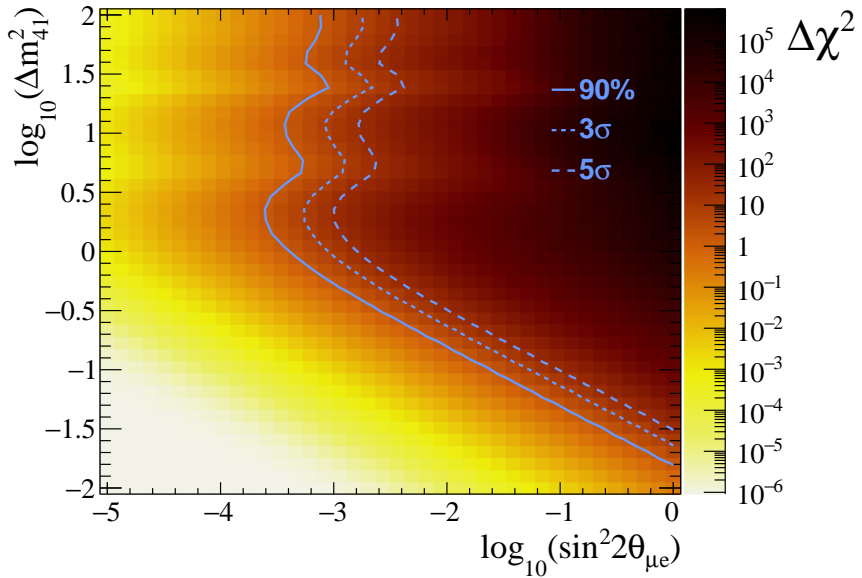


**Figure 1.12.:** The  $\nu_e$  appearance  $\chi^2$  surface from fits including flux and interaction systematics. Contours of constant  $\chi^2$  values which correspond to 90%,  $3\sigma$  and  $5\sigma$  confidence levels have been overlayed onto the surface.

When producing sensitivity contours, the fits may be generated for an individual detector as well as any combination of multiple detectors. The left plot of Figure 1.13 shows the  $\nu_e$  appearance statistical-only sensitivity contours from each individual detector as well as all possible combinations (the black curve labelled "SBN" refers to a contour from combining all three detectors). It can be seen that for large  $\Delta m_{41}^2$  (greater than  $\sim 5 \text{ eV}^2$ ), that the SBND detector dominates the sensitivity whereas for small  $\Delta m_{41}^2$  (less than  $\sim 0.7 \text{ eV}^2$ ) the ICARUS detector dominates. It should also be noted that only by combining the fits from all three detectors can the best sensitivities be obtained. Having this multi-detector design is one of the key advantages of the SBN program. The right plot of Figure 1.13 is akin to the left one, but with the inclusion of flux and interaction systematics in the fits. Again, the improvements to the sensitivity are highlighted by combining multiple detectors.

The previously discussed figures showing contours including systematic uncertainties simply included all the flux and interaction systematics outlined in Section ??, however, it is possible to apply only certain systematics at a time. The left plot

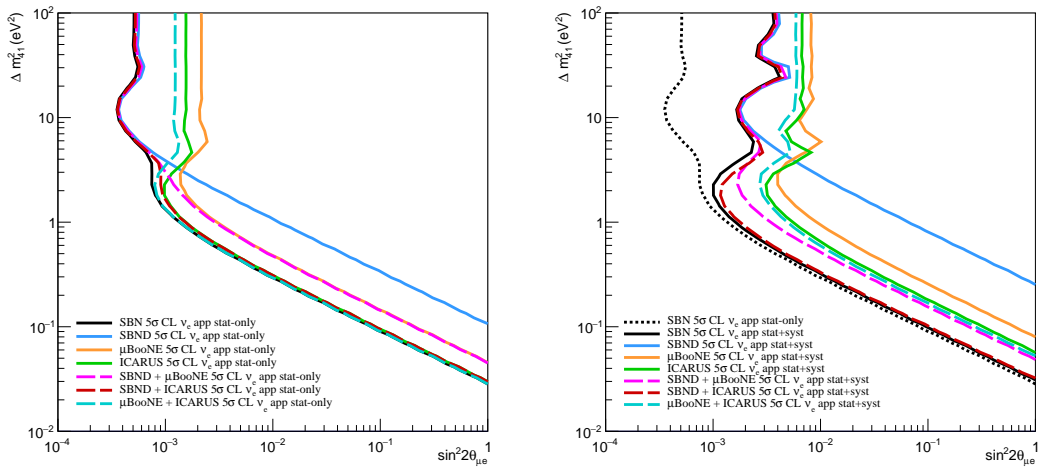


**Figure 1.13.:** Contributions to the SBN  $\nu_e$  appearance sterile oscillation sensitivity from each detector and combinations of detectors in the SBN program. The statistical-only plots in the left-hand figure show that SBND is most sensitive to the region  $\Delta m_{41}^2 > \sim 3$  eV<sup>2</sup> and ICARUS is most sensitive to  $\Delta m_{41}^2 < \sim 3$  eV<sup>2</sup>. The right-hand figure includes flux and interaction systematic parameters and highlights the considerable improvement in the oscillation sensitivity when including multiple detectors in the fits.

of Figure 1.14 shows the reduction in sensitivity when individually applying the flux, proposal interaction, modern interaction and all the interaction systematics compared to the statistical only case. This allows for the impact of the different systematic groups to be assessed. The right hand plot of Figure 1.14 shows the ratio of the exclusion contours to the statistical only case. This gives a clearer measure of the impact on the sensitivity in  $\sin^2 2\theta_{\mu e}$  space. It follows that the interaction systematics have the biggest impact on the sensitivity which in turn are dominated by the modern set of interaction parameters. The proposal set of interaction parameters have the smallest impact with the magnitude of the impact from the flux parameters being somewhere in between the two sets of interaction parameters.

The complete  $\nu_e$  appearance exclusion sensitivities and allowed regions for both the statistical only case and with the inclusion of flux and interaction systematics are shown in Figure 1.15 for the entire SBN program alongside external limits from the Liquid Scintillator Neutrino Detector (LSND) and Karlsruhe Rutherford

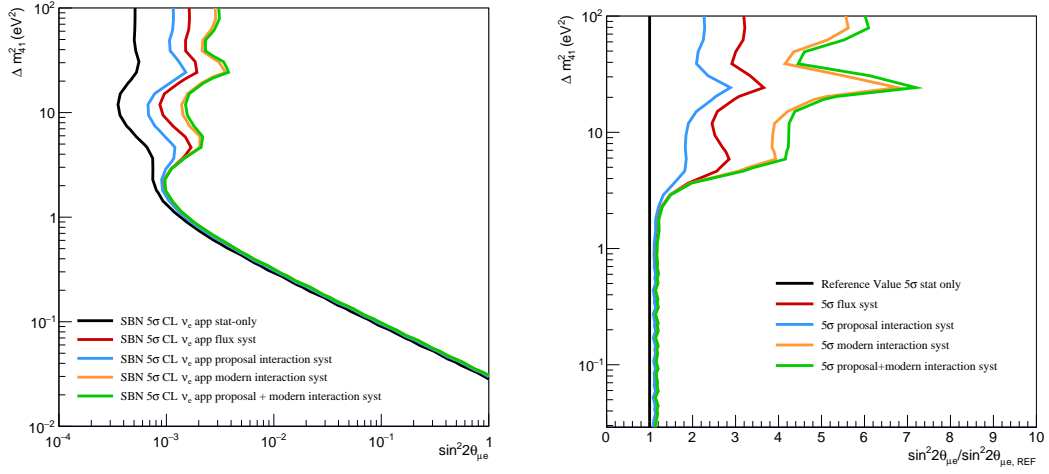


**Figure 1.14.:** The left plot shows the reduction in sensitivity from the stat-only contour when including each set of systematic parameters in the fits and was produced by the VALOR fitting framework. The right plot shows the relative location of each systematic contour in  $\sin^2 2\theta_{\mu e}$  space, with respect to the statistical-only case for the active region of  $\Delta m_{41}^2$  phase space.

Medium Energy Neutrino (KARMEN) experiments [5]. For comparison purposes, it should be noted that the contours produced for the SBN program are at the  $5\sigma$  confidence level whereas the results from both LSND and KARMEN are at the 99% confidence level. The results from SBN shows an improvement over the KARMEN results for essentially all  $\Delta m_{41}^2$  values and the allowed region is largely consistent with the LSND result.

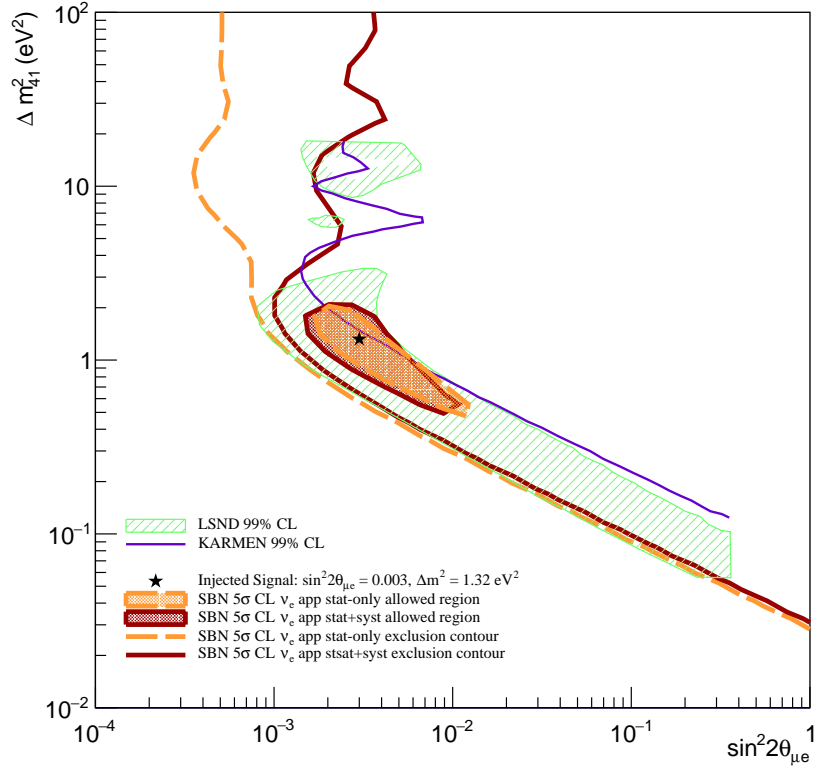


**Figure 1.15.:**  $\nu_e$  appearance exclusion contours and allowed regions for the stat only case and with flux and interaction systematic uncertainties included. External limits from the LSND and KARMEN experiments have been overlayed [5]. (The confidence intervals for each contour are shown in the legend and it should be noted that those from external limits are not the same as those from the contours produced for the SBN program.)

### 1.3.2. $\nu_e$ Disappearance Analysis

Mirroring the  $\nu_e$  appearance channel, the  $\nu_e$  disappearance channel observes a reduction in the nominal  $\nu_e$  event rate. This is shown in Figure 1.16 where the integrated spectrum produced with oscillation parameters  $\sin^2 2\theta_{ee} = 0.4$  and  $\Delta m_{41}^2 = 3 \text{ eV}^2$  has been overlayed onto the breakdown of the nominal spectrum for each of the three detectors. As is the case for  $\nu_e$  appearance, the oscillation signal is relatively small in SBND whereas both MicroBooNE and ICARUS observe a much more significant signal.

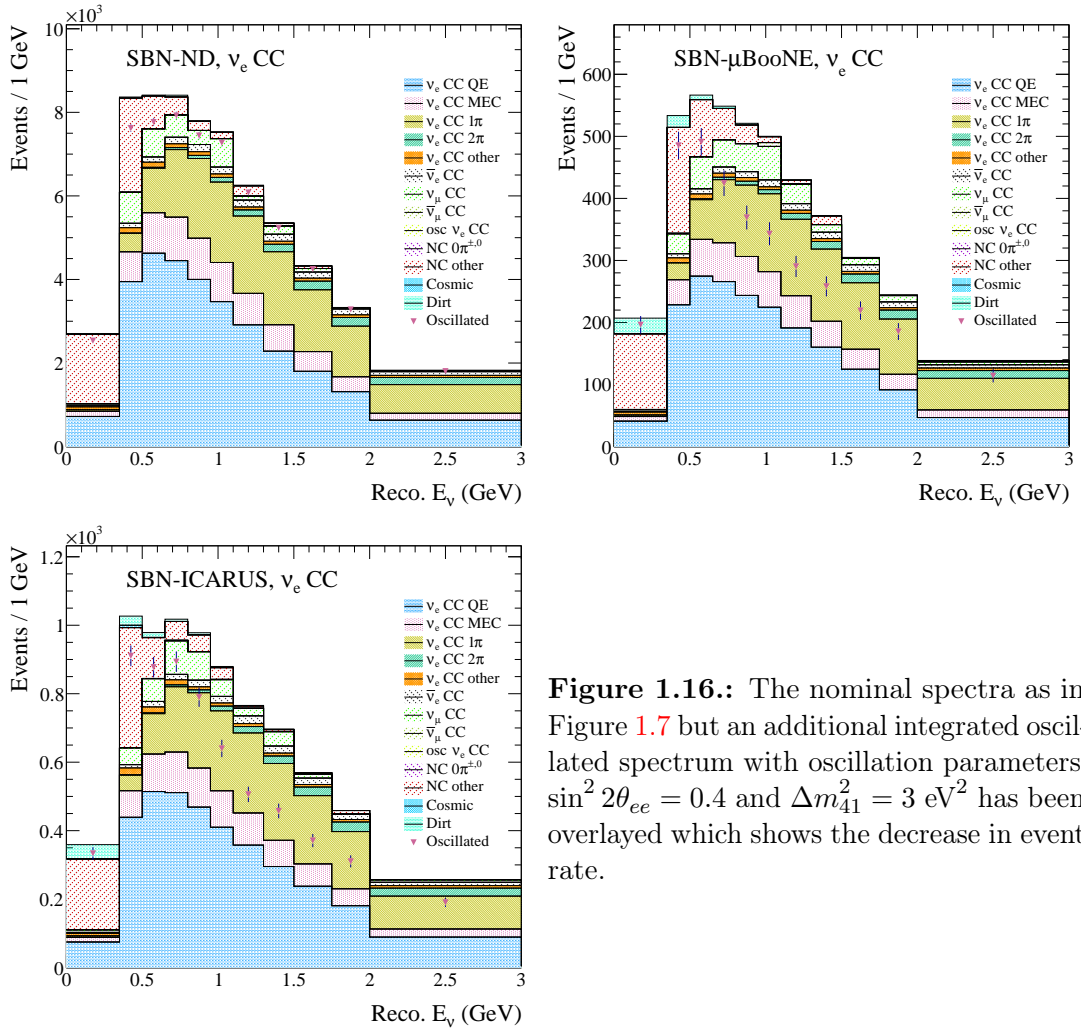


**Figure 1.16.:** The nominal spectra as in Figure 1.7 but an additional integrated oscillated spectrum with oscillation parameters,  $\sin^2 2\theta_{ee} = 0.4$  and  $\Delta m_{41}^2 = 3 \text{ eV}^2$  has been overlayed which shows the decrease in event rate.

The top left plot of Figure 1.17 shows the  $\nu_e$  disappearance stat only exclusion contour and allowed region from fits combining all three SBN detectors. The injected point  $\Delta m_{41}^2 = 3 \text{ eV}^2$ ,  $\sin^2 2\theta_{\mu e} = 0.4$ , used when producing the allowed region is shown along with two further points on the exclusion contour at  $\Delta m_{41}^2 = 1 \text{ eV}^2$ ,  $\sin^2 2\theta_{\mu e} = 0.29$  and  $\Delta m_{41}^2 = 100 \text{ eV}^2$ ,  $\sin^2 2\theta_{\mu e} = 0.085$ .  $\nu_e$  disappearance spectra are produced using oscillation parameters corresponding to each of these three points for each of the three SBN detectors. The ratio of each of these oscillated spectra to the nominal for each detector are shown in the the remaining plots in Figure 1.17 and highlight the expected oscillation signal.

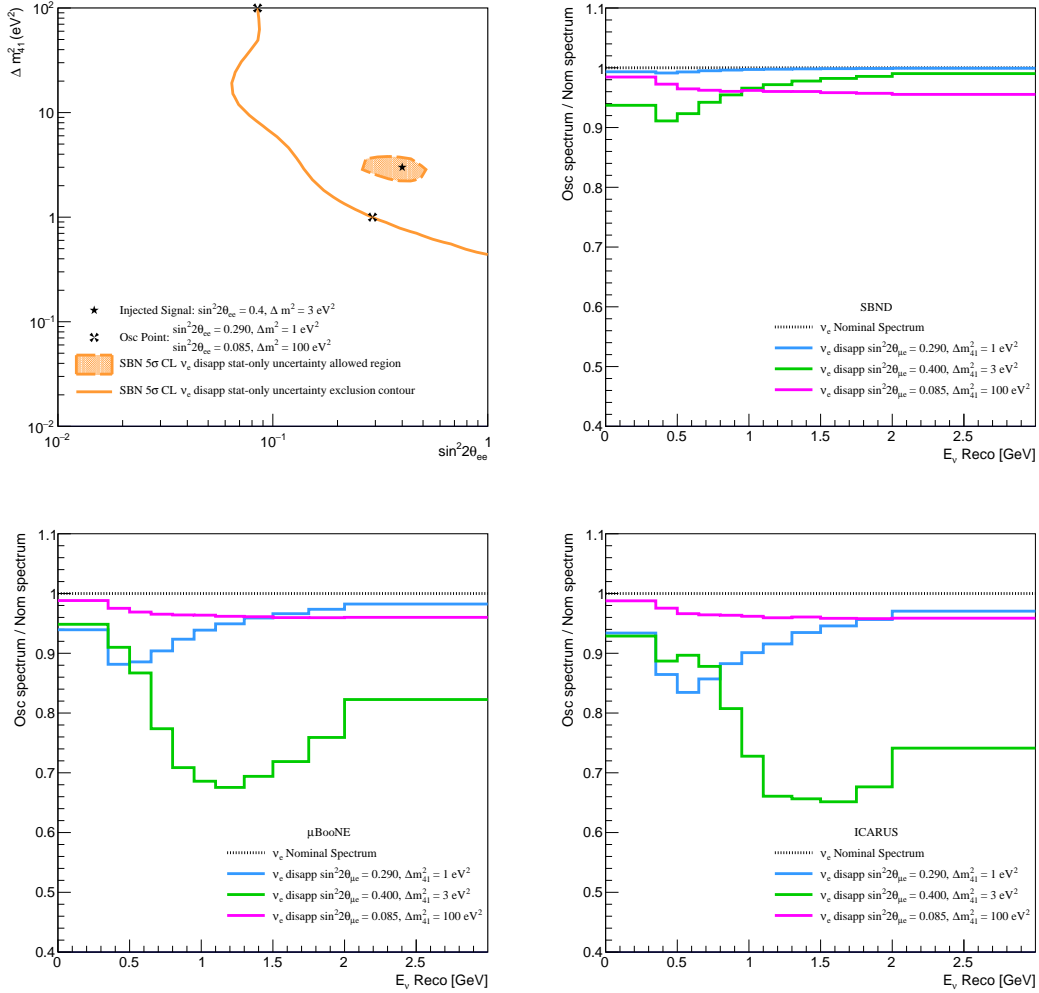


**Figure 1.17.:**  $\nu_e$  disappearance stat-only exclusion contour and allowed region. The injected point at  $\sin^2 2\theta_{ee} = 0.4$ ,  $\Delta m_{41}^2 = 3 \text{ eV}^2$  used for the allowed region is shown along with two further points at  $\sin^2 2\theta_{ee} = 0.29$ ,  $\Delta m_{41}^2 = 1 \text{ eV}^2$  and  $\sin^2 2\theta_{ee} = 0.085$ ,  $\Delta m_{41}^2 = 100 \text{ eV}^2$  (top left). The ratio of spectra with oscillation parameters corresponding to the three points mentioned versus nominal are shown for SBND (top right), MicroBooNE (bottom left) and ICARUS (bottom right).

Similar to Figure 1.13, Figure 1.18 shows the  $\nu_e$  disappearance sensitivity from individual detectors and combinations of multiple detectors for both the statistical-only case (Left) and the case with flux and interaction systematics (Right). Again, SBND dominates the sensitivity at high mass splitting whereas ICARUS

is dominant for low mass splitting with the emphasis being on the improvement to the overall sensitivity when fits from all three SBN detectors are combined.

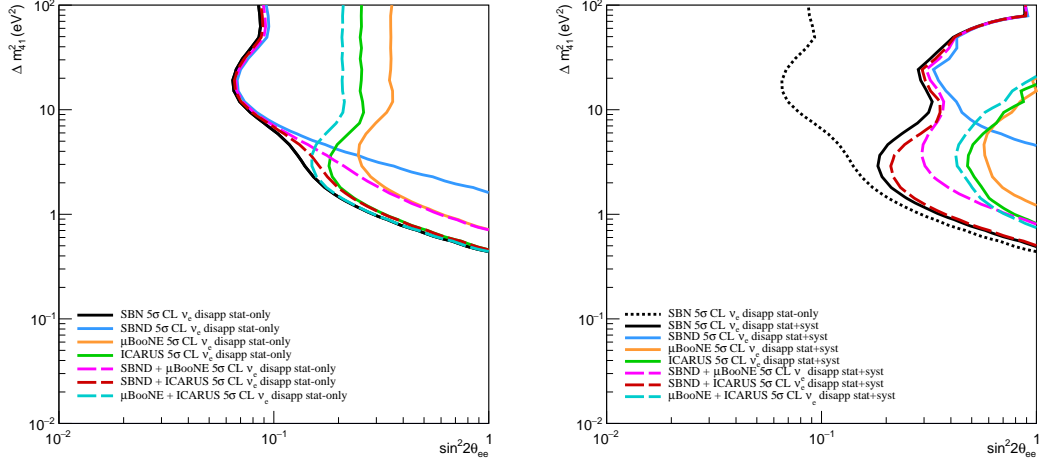


**Figure 1.18.:** Contributions to the SBN  $\nu_e$  disappearance sterile oscillation sensitivity from each detector and combinations of detectors in the SBN program produced. The statistical-only plots in the left-hand figure show that SBND is most sensitive to the region  $\Delta m_{41}^2 > 3$  eV $^2$  and ICARUS is most sensitive below  $\Delta m_{41}^2 < 3$  eV $^2$ . The right-hand figure includes flux and interaction systematic parameters and highlights the considerable improvement in the oscillation sensitivity when including multiple detectors in the fits.

The relative contribution of the different systematic groups to the overall exclusion contour for  $\nu_e$  disappearance is comparable to the  $\nu_e$  appearance case. The interaction systematics again have the largest impact the majority of which is due to the modern set of parameters. The proposal set of parameters have the smallest impact with the magnitude of the impact from the flux parameters being somewhere in between the two sets of interaction parameters.

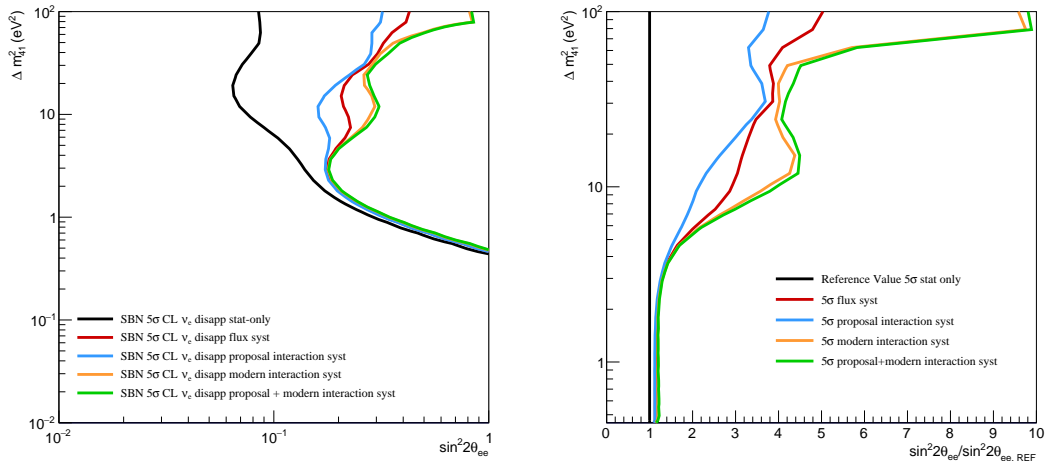


**Figure 1.19.:** The left plot shows the reduction in sensitivity from the stat-only contour when including each set of systematic parameters in the fits. The right plot shows the relative location of each systematic contour in  $\sin^2 2\theta_{ee}$  space, with respect to the statistical-only case for the active region of  $\Delta m_{41}^2$  phase space.

The complete  $\nu_e$  disappearance exclusion sensitivities and allowed regions for both the statistical only case and with the inclusion of flux and interaction systematics are shown in Figure 1.20 for the entire SBN program alongside external limits from the ND280 detector which serves as one of the near detectors as part of the T2K experiment [6]. The results for the SBN program are shown at a 5 $\sigma$  confidence level whereas the allowed region from the T2K experiment is shown at both 68% and 90% confidence level and the exclusion contour is at a 95% confidence level [7]. The results from SBN exclude a substantial portion of the T2K allowed region with the exclusion limits at high  $\Delta m_{41}^2$  not being as strong for the current comparison.

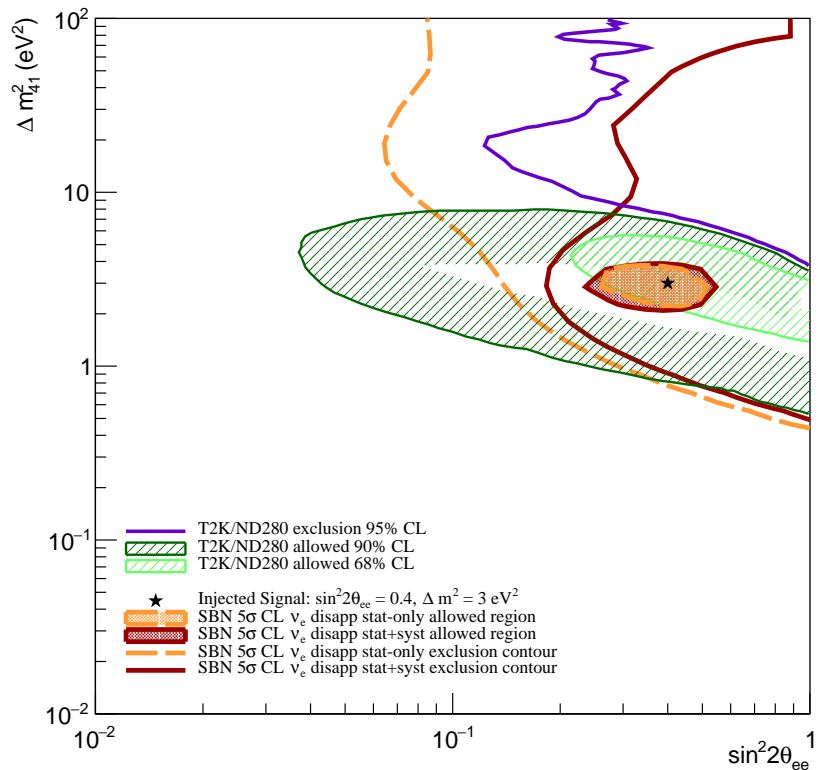


**Figure 1.20.:**  $\nu_e$  disappearance exclusion contours and allowed regions for the stat only case and with flux and interaction systematic uncertainties included. External limits from the T2K experiments have been overlayed [7]. (The confidence intervals for each contour are shown in the legend and it should be noted that those from external limits are not the same as those from the contours produced for the SBN program.)

### 1.3.3. $\nu_e$ Sensitivities Based on Shower Energy Reconstruction

The reconstructed neutrino energy used in the analyses shown so far is based on truth information where smearing has been applied to emulate a reconstructed value.

To better motivate the reconstructed energy used, the results from Chapter ?? have been used to tweak the true energy of the showering particles (electrons or photons) to emulate a reconstructed energy based on the reconstruction performance that has been observed with the currently available tools. Since only the reconstructed shower energy was actively investigated here, any non-showering particles continue to have their reconstructed energy estimated by directly smearing the true energy.

The two cases considered for estimating the reconstructed energy of the showering particle are,

- A flat negative bias of 20% is applied to the true energy for all particles.
- A flat negative bias applied to the true energy along with an additional variation to emulate the resolution of the reconstruction performance. The magnitude of the bias and the width of the resolution are functions of the true energy. The resolution was emulated by randomly choosing a number based on a Gaussian with a given standard deviation. The three categories used depending on the true energy are shown in Table 1.6.

E [MeV]	Bias	$\sigma$
$E < 100$	40%	0.15
$100 \leq E < 200$	30%	0.125
$E > 200$	20%	0.1

**Table 1.6.:** The variable bias and resolution used to emulate reconstructed energy.

The simplistic approach of applying a flat 20% bias was motivated by the conservative results from Figure ?? which shows that the typical bias is of order 20%. The more involved process of applying an energy dependent bias and resolution

are motivated by Figure ???. It can be seen that above energies of  $\sim 200$  MeV, the bias and standard deviation remain fairly constant, but at energies below this, the bias and resolution increase as the energy decreases.

The full  $\nu_e$  event selection as described in Section ?? was repeated but with the above changes applied. The events from these selections were then used to produce exclusion contours using the same systematic uncertainties as previously described. The overall event rate from the selections using the reconstructed information motivated by Chapter ?? is lower than than the traditional method which relied on energy smearing.

The exclusion contours comparing the three selections are shown on the left of Figure 1.21 and Figure 1.22 for  $\nu_e$  appearance and disappearance respectively. The difference between the three exclusion contours is relatively minor and therefore the ratios of the contours to the contour from the original selection are shown on the right of their respective figures. Since the event rate is reduced in the updated selections, it is expected that the overall exclusion sensitivity would also be reduced. This indeed the case for most values of  $\Delta m_{41}^2$  with only a couple of areas where the selection with the flat 20% bias appears to improve the sensitivity.

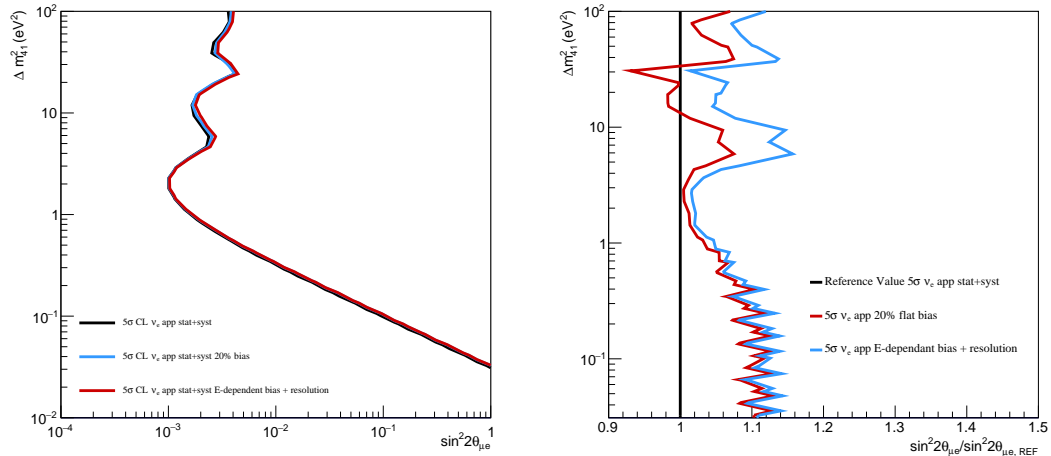


**Figure 1.21.:** Left:  $\nu_e$  appearance exclusion contours with flux and interaction uncertainties using events from the original selection and the ones motivated by results from electromagnetic (EM) shower reconstruction. Right: The ratio of the exclusion contours to the contour from the original selection.

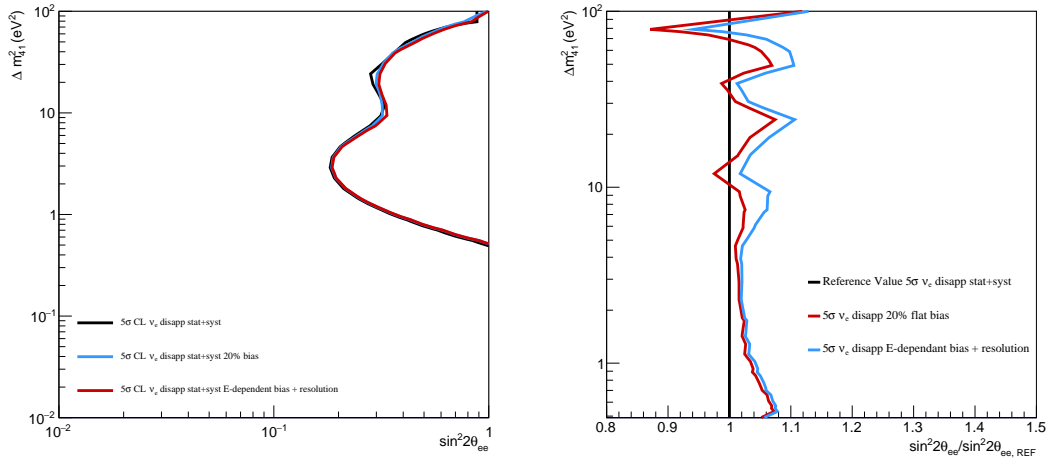


**Figure 1.22.:** Left:  $\nu_e$  disappearance exclusion contours with flux and interaction uncertainties using events from the original selection and the ones motivated by results from EM shower reconstruction. Right: The ratio of the exclusion contours to the contour from the original selection.

#### 1.4. $\nu_\mu$ Disappearance Analysis

looks a bit out of place

A similar analysis and validation to that described in Section 1.2 and Section 1.3 was performed for the two  $\nu_e$  channels was also done for the  $\nu_\mu$  disappearance channel.

The nominal event rate breakdown for each of the detectors is shown in Figure 1.23 where an integrated spectrum with oscillation parameters  $\sin^2 2\theta_{\mu\mu} = 0.072$ ,  $\Delta m_{41}^2 = 1.32 \text{ eV}^2$  has been overlayed. The overall magnitude of the event rate is several order of magnitude greater than that for  $\nu_e$  owing to the fact that the Booster Neutrino Beam (BNB) consists predominantly of  $\nu_\mu$ . As was the case for  $\nu_e$  disappearance, the reduction in events for SBND is relatively small whereas for MicroBooNE and ICARUS it is much more significant.

The complete  $\nu_\mu$  disappearance exclusion sensitivities and allowed regions for both the statistical only case and with the inclusion of flux and interaction systematics are shown in Figure 1.24 for the entire SBN program alongside external limits from Main Injector Neutrino Oscillation Search (MINOS) and its successor MINOS+, combined results from SciBar Booster Neutrino Experiment (SciBooNE) and Mini

Booster Neutrino Experiment (MiniBooNE) and the IceCube experiment [8] [9] [10]. The results for the SBN program are shown at a  $5\sigma$  confidence level whereas the exclusion region from the MINOS/MINOS+, SciBooNE/MiniBooNE and IceCube experiments are shown at the 90% confidence. The IceCube experiment also shows an allowed region at the 99% confidence level. The results from SBN show a stronger sensitivity to that obtained by MiniBooNE/SciBooNE for all mass splitting values. The exclusion contour is also comparable to that from MINOS/MINOS+ for  $\Delta m_{41}^2 \gtrsim 1 \text{ eV}^2$ , however below this value MINOS/MINOS+ provides a stronger limit. The exclusion contour from IceCube again provides a stronger limit at  $\Delta m_{41}^2 \lesssim 1 \text{ eV}^2$ , but for higher values, SBN expects to improve on the results from IceCube. The allowed region from IceCube intersect the one from SBN so they aren't fully compatible.

For a complete discussion of the  $\nu_\mu$  disappearance channel, see [12].

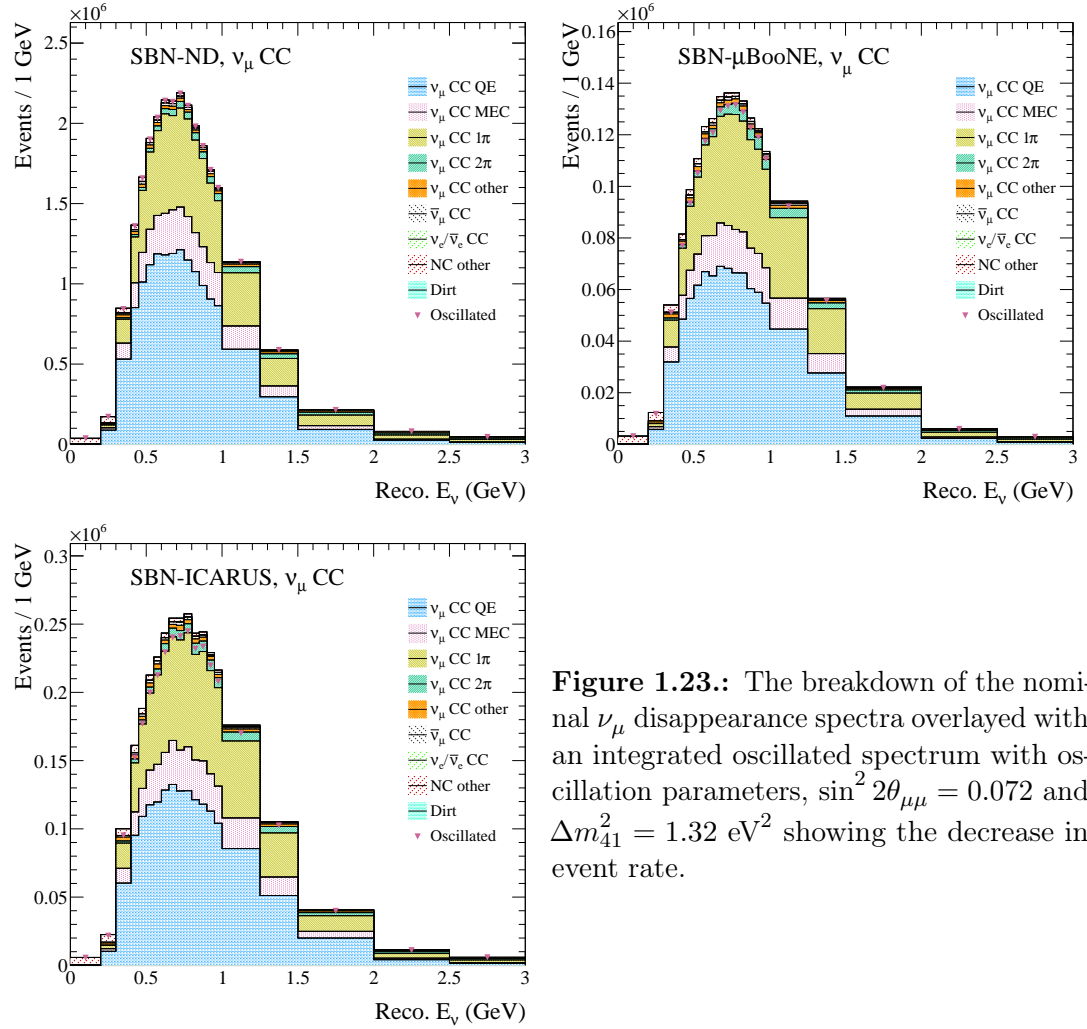


**Figure 1.23.:** The breakdown of the nominal  $\nu_\mu$  disappearance spectra overlayed with an integrated oscillated spectrum with oscillation parameters,  $\sin^2 2\theta_{\mu\mu} = 0.072$  and  $\Delta m_{41}^2 = 1.32 \text{ eV}^2$  showing the decrease in event rate.

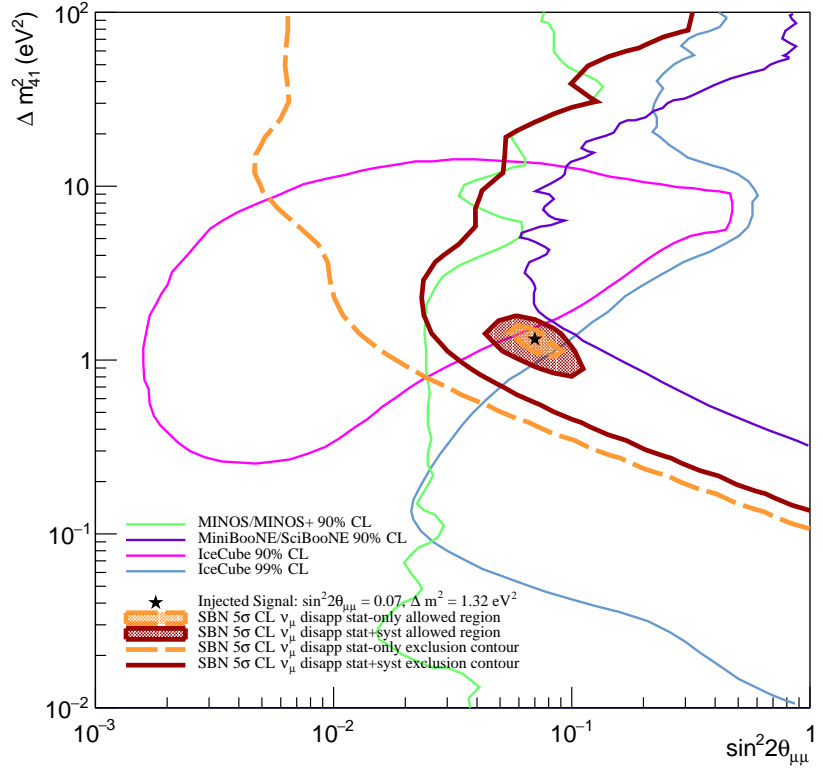


**Figure 1.24.:**  $\nu_\mu$  disappearance exclusion contours and allowed regions for the stat only case and with flux and interaction systematic uncertainties included. External limits from the MINOS/MINOS+, MiniBooNE/SciBooNE and IceCube experiments have been overlayed [11] [9] [10]. (The confidence intervals for each contour are shown in the legend and it should be noted that those from external limits are not the same as those from the contours produced for the SBN program.)

By now, I'm starting to get lost. Too many plots / sensitivities, but the structure is not helping create a clear narrative.

## 1.5. Additional Efficiency and Energy Scale

### Systematics

As was mentioned in Section ??, efficiency systematics are not currently included in the *standard* analyses. In order to get a measure of the possible impact of efficiency systematics on the sensitivity, various covariance matrices were produced following the scheme outlined in Section ??.

Matrices were produced to investigate the impact of;

1. Fully correlated errors only.
2. Various combinations of uncorrelated errors with a fixed correlated error.
3. Uncorrelated errors only applied to a single detector at a time.
4. A poorly constrained uncorrelated error on a single set of bins.

Unless otherwise stated, the uncertainties from efficiency covariance matrices are applied in addition to the flux and interaction systematics.

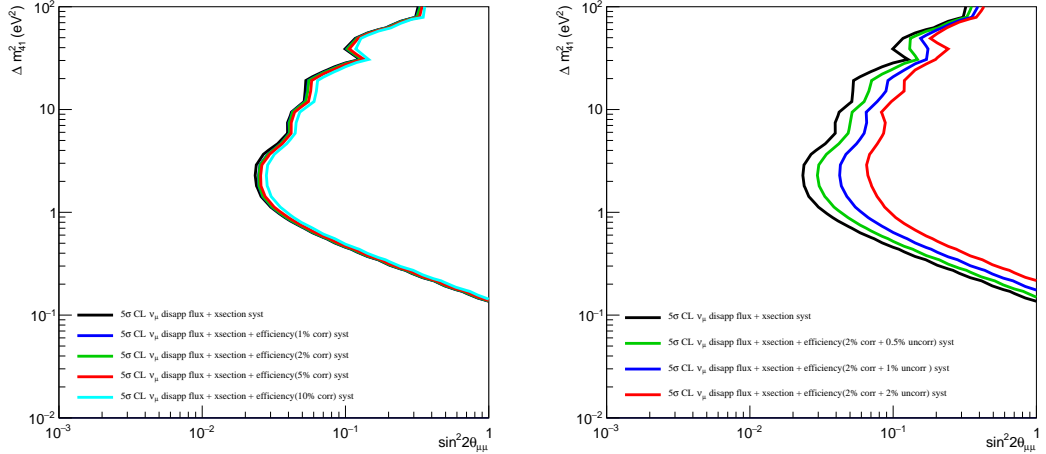
The study of the impact of different efficiency uncertainties was first done for the  $\nu_\mu$  channel because it was expected that there would be a greater impact than for either of the  $\nu_e$  channels. This is because the typical event rate for the  $\nu_\mu$  channel is several orders of magnitude greater than that of  $\nu_e$  meaning that the  $\nu_\mu$  channel is systematics limited whereas the  $\nu_e$  channels may tend towards being statistics limited. Once a contour becomes statistics limited, continuing to apply additional systematic uncertainties will begin to have diminishing impacts.

#### 1.5.1. Impact of Efficiency Systematics on $\nu_\mu$

##### Disappearance Sensitivities

The impact of fully correlated uncertainties up to 10% are shown on the left of Figure 1.25 whilst keeping the uncorrelated uncertainty at 0%. The right plot shows the impact of increasing the uncorrelated uncertainties uniformly across all bins with a fixed correlated uncertainty of 2%. It follows that for even relatively

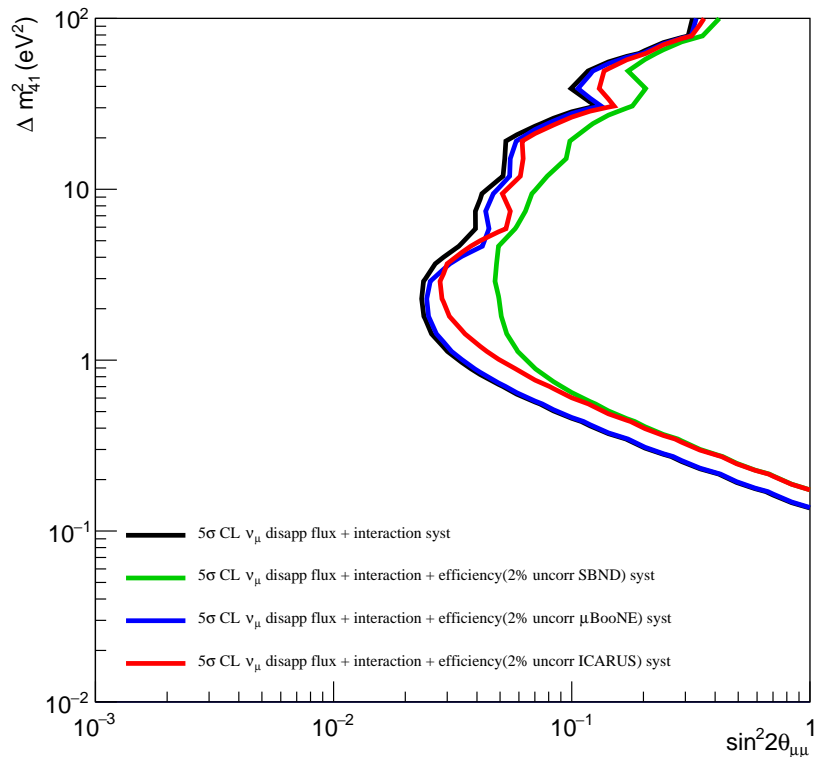
large correlated uncertainties the impact on the sensitivity is minor and that any reduction in sensitivities will be largely dominated by the uncorrelated uncertainty.



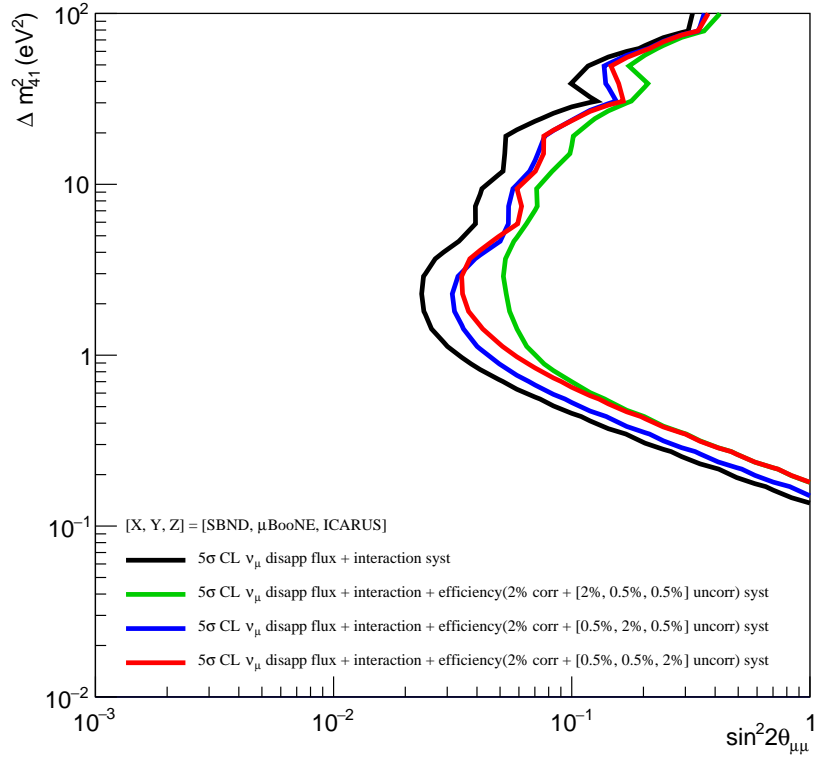
**Figure 1.25.:** The impact on the  $\nu_\mu$  disappearance exclusion sensitivity by applying fully correlated uncertainties ranging from 1% to 10% to all bins (Left) and by applying a fixed 2% fully correlated uncertainty with additional uncorrelated uncertainty ranging from 0.5% to 2% across all bins (Right).

Figure 1.26 shows the impact of applying a 2% uncorrelated uncertainty only to each of the SBN detectors one at a time. The MicroBooNE detector has a minor impact at around  $\Delta m_{41}^2 = 10 \text{ eV}^2$  and close to no impact at small and large  $\Delta m_{41}^2$  values. The ICARUS detector has a larger impact for most  $\Delta m_{41}^2$  values but again only has a minor contribution at very large  $\Delta m_{41}^2$  values. Across most  $\Delta m_{41}^2$  values greater than  $\sim 0.5 \text{ eV}^2$ , SBND dominates the sensitivity. At values below  $0.5 \text{ eV}^2$  the reduction in sensitivity due to SBND and ICARUS are comparable. This point is emphasised in Figure 1.27 where the fully correlated uncertainty is fixed at 2% and the uncorrelated uncertainty is set to 2% for one of the three SBN detectors whilst being set to 0.5% for the other two detectors. The contour where SBND's uncorrelated uncertainty is set to 2% looks similar to the corresponding contour in Figure 1.26. It has been shown that the uncorrelated component of the uncertainty has a large impact when compared to the correlated component and that any efficiency uncertainties impact SBND more than the other two detectors so this result ought to be expected. Similarly, the two contours

where uncorrelated uncertainty is set to 2% for MicroBooNE and ICARUS are pulled towards the SBND contour since despite it having a smaller associated uncorrelated uncertainty, it will still contribute significantly.



**Figure 1.26.:** The impact on the  $\nu_\mu$  disappearance exclusion sensitivity by applying a 2% uncorrelated efficiency uncertainty to a single one of the three SBN detectors.



**Figure 1.27.:** The impact on the  $\nu_\mu$  disappearance exclusion sensitivity by applying a 2% fully correlated efficiency uncertainty for each of the SBN detectors and a 2% uncorrelated uncertainty for one of the detectors and a 0.5% uncorrelated uncertainty for the other two detectors. This is repeated for each of the detectors. The associated covariance matrix used for the case where SBNDs uncorrelated uncertainty was set to 2% is shown in the bottom left plot of Figure ??.

Instead of exploring the impact from fully uncorrelated uncertainties or a constant uncorrelated uncertainty across all bins in a detector, Figure 1.28 considers the case where a single set of bins are poorly constrained. The sets of bins considered are,

- CC signal below the peak energy ( $< 0.6$  GeV),
- CC signal at the peak energy ( $[0.6 - 1.0]$  GeV),
- CC signal above the peak energy ( $> 1.0$  GeV),

- Background.

In each case, the uncorrelated uncertainty for the bins of interest are set to 2% in each of the SBN detectors, whilst the rest of the uncorrelated uncertainties are set to 0.5% and the fully correlated uncertainty is fixed at 2%. Increasing the uncertainty associated with the background bins has the smallest impact whereas increasing the uncertainty for the high and low energy bins has the largest impact at large and small  $\Delta m_{41}^2$  respectively. The peak energy bins also contribute significantly around  $\Delta m_{41}^2$  equal to 1 eV<sup>2</sup> and 10 eV<sup>2</sup>.

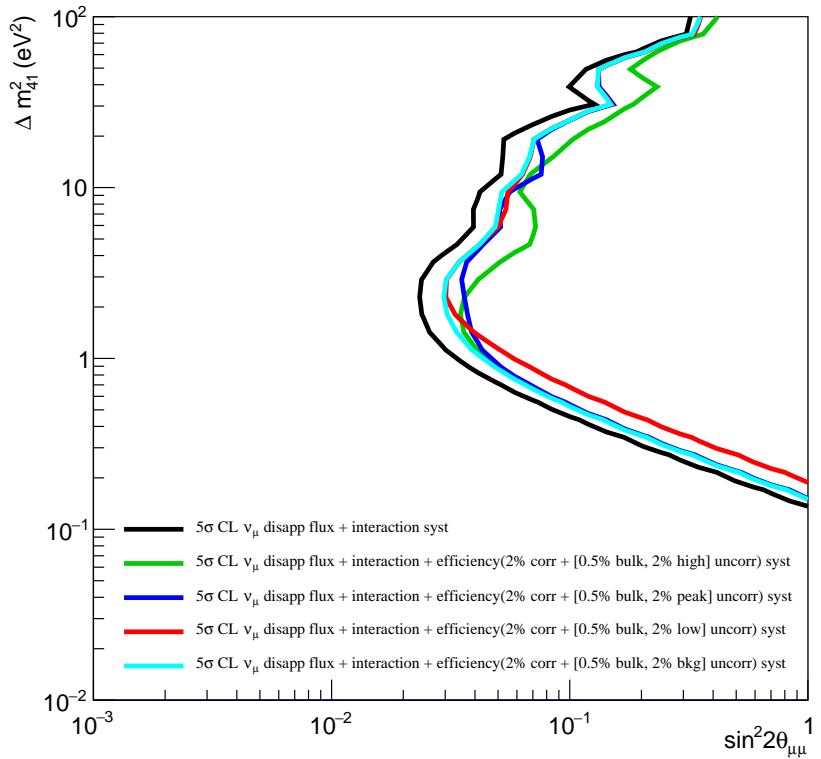


**Figure 1.28.:** The impact on the  $\nu_\mu$  disappearance exclusion sensitivity by applying a 2% fully correlated efficiency uncertainty for each of the SBN detectors and a 0.5% uncorrelated uncertainty for all but a single set of bins where the uncorrelated uncertainty is set to 2%. The 'peak' energy bins are defined as those covering an energy range of [0.6, 1.0] GeV. The 'high' and 'low' energy bins are defined as those covering energies above and below the peak energy respectively and the 'bkg' bins are all the bins associated with background events. The set of bins of interest are applied to each of the three detectors and the covariance matrix for where the peak energy bins are the ones in question is shown in the bottom right plot of Figure ??.

### 1.5.2. Impact of Efficiency Systematics on $\nu_e$ Appearance Sensitivities

In order to gauge the contribution of some typical efficiency uncertainty, Figure 1.29 shows the impact on the  $\nu_e$  appearance sensitivity from individual sets of systematic parameters as in Figure 1.14 but with the addition of a 2% correlated + 2% uncorrelated efficiency uncertainty. The impact of the efficiency uncertainty is comparable to the proposal interaction systematics having the smallest contribution to the sensitivity.

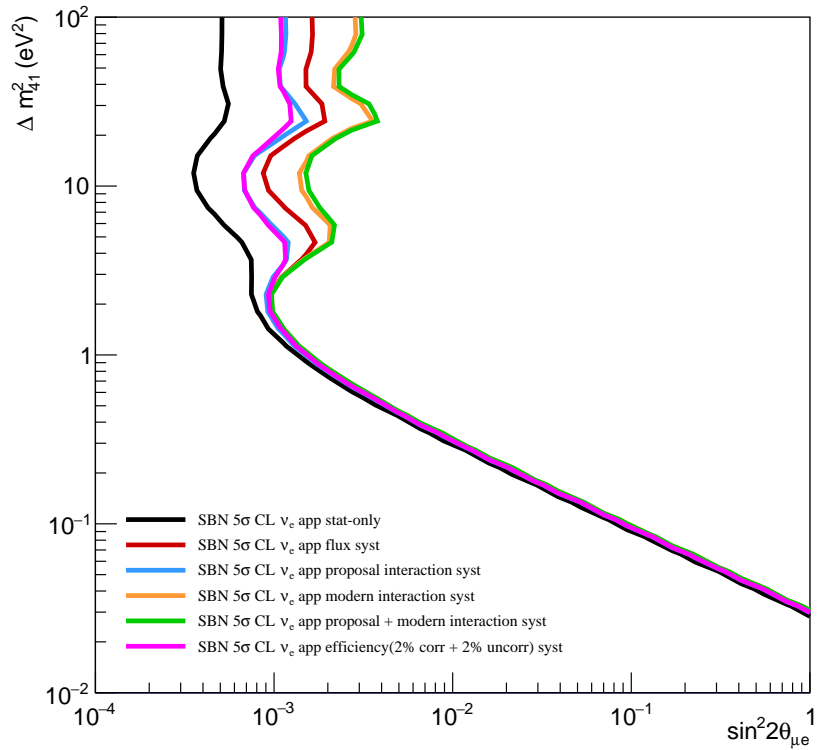


**Figure 1.29.:** The reduction in the  $\nu_e$  appearance sensitivity from the stat-only contour when including each set of systematic parameters in the fits. Similar to Figure 1.14 but with the addition of a 2% correlated and 2% uncorrelated efficiency uncertainty.

The reduction in sensitivity from applying a 10% correlated uncertainty and a 2% correlated + 2% uncorrelated uncertainty are shown in Figure 1.30. Since a

correlated error of 10% has a close to negligible impact, the results from applying correlated uncertainties less than 10% as was done for the  $\nu_\mu$  channel have been omitted. Similarly, applying smaller uncorrelated uncertainties would again only have a minor impact so these have also been omitted.

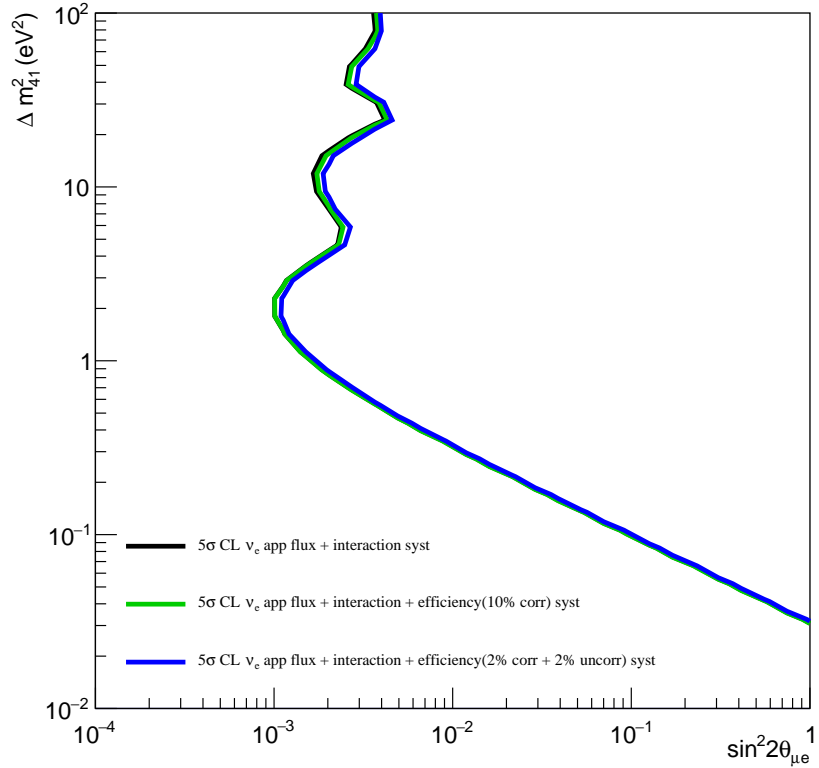


**Figure 1.30.:** The impact on the  $\nu_e$  appearance exclusion sensitivity by applying a 10% fully correlated efficiency uncertainty to all bins and by applying 2% fully correlated + 2% uncorrelated efficiency uncertainty.

Figure 1.31 asses the impact of a 2% uncorrelated uncertainty which is applied to each detector one at a time. Applying the uncertainty to MicroBooNE and ICARUS appears to have a negligible impact across all  $\Delta m_{41}^2$  values. SBND has a relatively small impact at high  $\Delta m_{41}^2$  values which resembles the loss in sensitivity that was seen by applying a 2% correlated + 2% uncorrelated uncertainty across all bins in Figure 1.30. It follows that any reduction in sensitivity due to efficiency uncertainties is driven by SBND. Since SBND is most sensitive to large  $\Delta m_{41}^2$

values and has higher statistics than MicroBooNE and ICARUS, the results are consistent with the idea that  $\nu_e$  channel is close to becoming statistics limited.

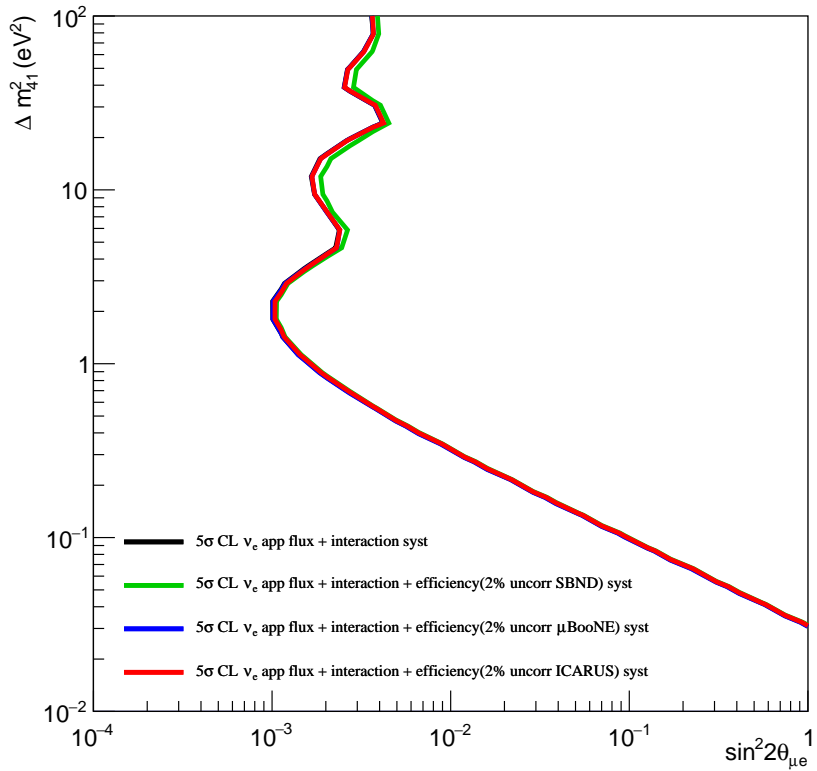


**Figure 1.31.:** The impact on the  $\nu_e$  appearance exclusion sensitivity by applying a 2% uncorrelated efficiency uncertainty to a single one of the three SBN detectors.

The impact of having a set of bins with a poorly constrained uncertainty was also studied using the same scheme that was outlined for the  $\nu_\mu$  case. Similar results were observed and are shown in Figure 1.32, albeit the change in sensitivity is much less prominent than for the  $\nu_\mu$  case. The background and low energy bins have the smallest impact with almost no visible difference whereas the peak and high energy bins do show some small reduction in the sensitivity.

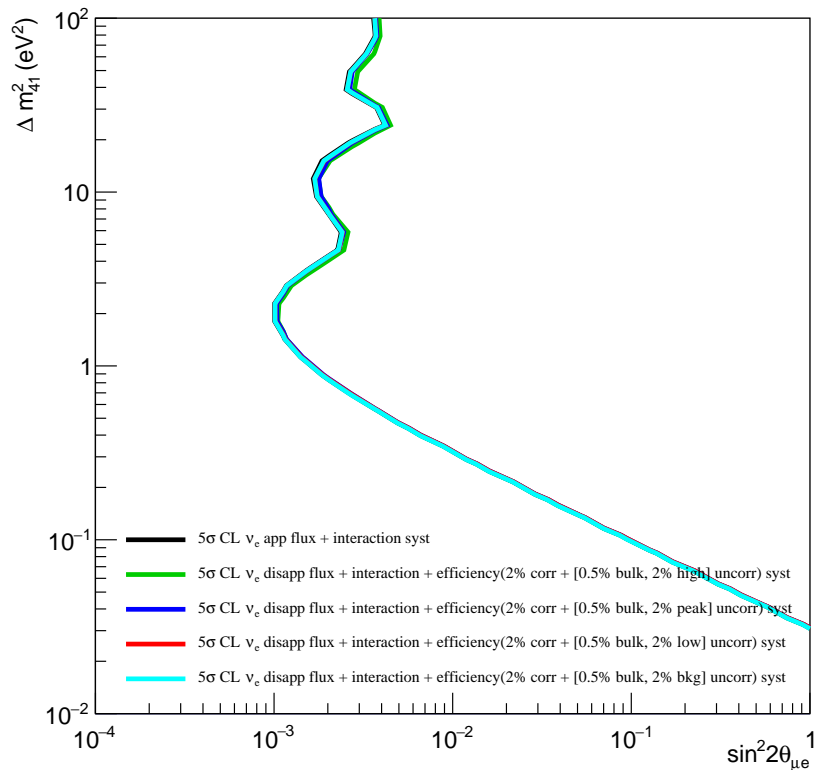


**Figure 1.32.:** The impact on the  $\nu_e$  appearance exclusion sensitivity by applying a 2% fully correlated efficiency uncertainty for each of the SBN detectors and a 0.5% uncorrelated uncertainty for all but a single set of bins where the uncorrelated uncertainty is set to 2%. The 'peak' energy bins are defined as those covering an energy range of [0.6, 1.0] GeV. The 'high' and 'low' energy bins are defined as those covering energies above and below the peak energy respectively and the 'bkg' bins are all the bins associated with background events. The set of bins of interest are applied to each of the three detectors.

### 1.5.3. Impact of Efficiency Systematics on $\nu_e$ Disappearance Sensitivities

As was done for  $\nu_e$  appearance, Figure 1.33 shows the impact from  $\nu_e$  disappearance sensitivity from individual sets of systematic parameters as in Figure 1.19 but with the addition of a 2% correlated + 2% uncorrelated efficiency uncertainty. The efficiency uncertainty shows the smallest reduction in sensitivity across all ranges of  $\Delta m_{41}^2 \gtrsim 3$  and is comparable to the other systematic sets at  $\Delta m_{41}^2$  values below  $\sim 3$ .

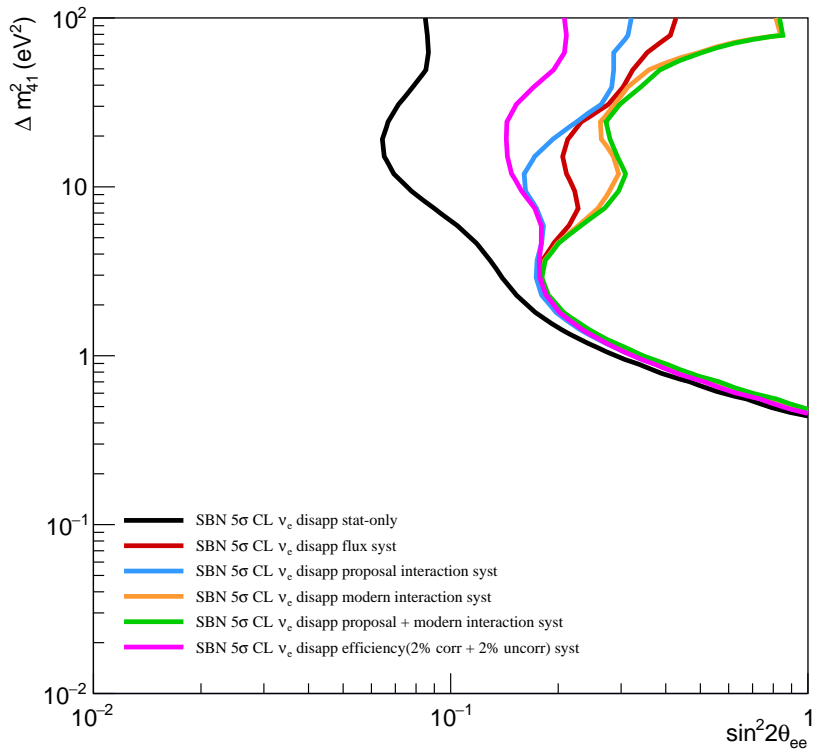


**Figure 1.33.:** The reduction in the  $\nu_e$  disappearance sensitivity from the stat-only contour when including each set of systematic parameters in the fits. Similar to Figure 1.19 but with the addition of a 2% correlated and 2% uncorrelated efficiency uncertainty.

Mirroring what was done for  $\nu_e$  appearance, Figure 1.34 shows the impact of applying a 10% correlated error and a 2% correlated + 2% uncorrelated error. The

correlated error again has an almost negligible impact and whilst the uncorrelated error has a larger impact it is still relatively small.

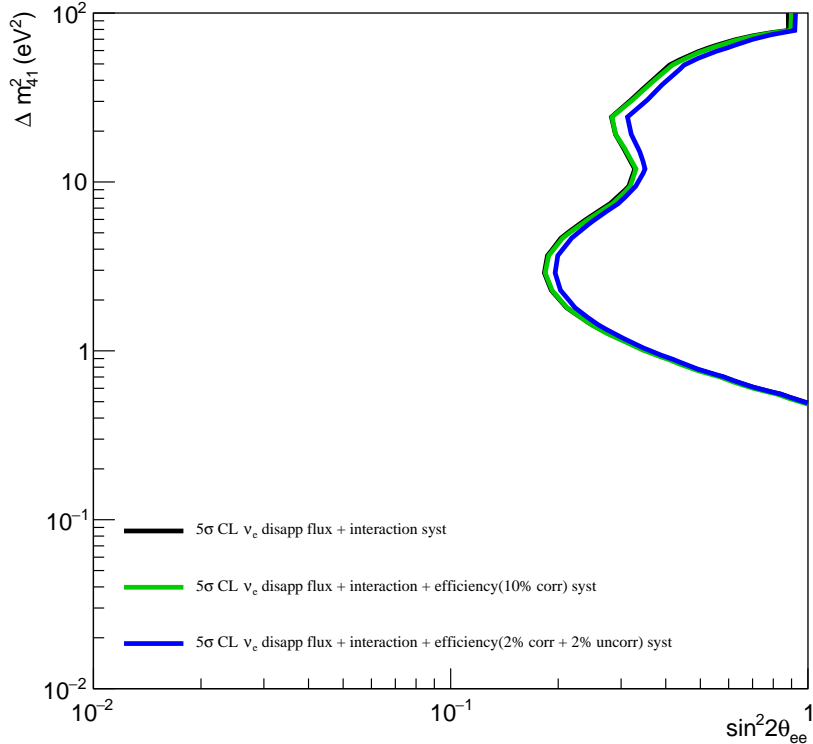


**Figure 1.34.:** The impact on the  $\nu_e$  disappearance exclusion sensitivity by applying a 10% fully correlated efficiency uncertainty to all bins and by applying 2% fully correlated + 2% uncorrelated efficiency uncertainty.

A 2% uncorrelated uncertainty is then applied to each detector one at a time. Figure 1.35 shows that majority of the reduction is due to SBND at above  $\Delta m_{41}^2 \sim 10$  (where SBND is dominant). Both MicroBooNE and ICARUS only have a minimal impact for any  $\Delta m_{41}^2$  values. This is consistent with what is shown in Figure 1.34.

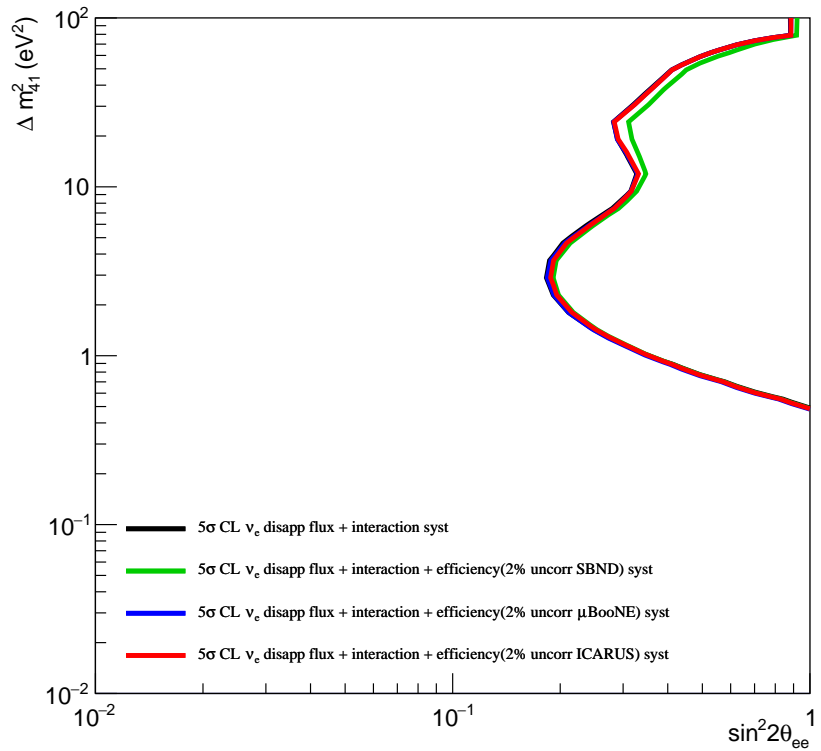


**Figure 1.35.:** The impact on the  $\nu_e$  disappearance exclusion sensitivity by applying a 2% uncorrelated efficiency uncertainty to a single one of the three SBN detectors.

Finally, the impact of having a set of poorly constrained bins is investigated in Figure 1.36. Similar to the  $\nu_e$  appearance case, the low energy and background bins only have a minimal impact, whereas the peak and high energy bins show a slightly larger impact but far less prominent than for the  $\nu_\mu$  channel.

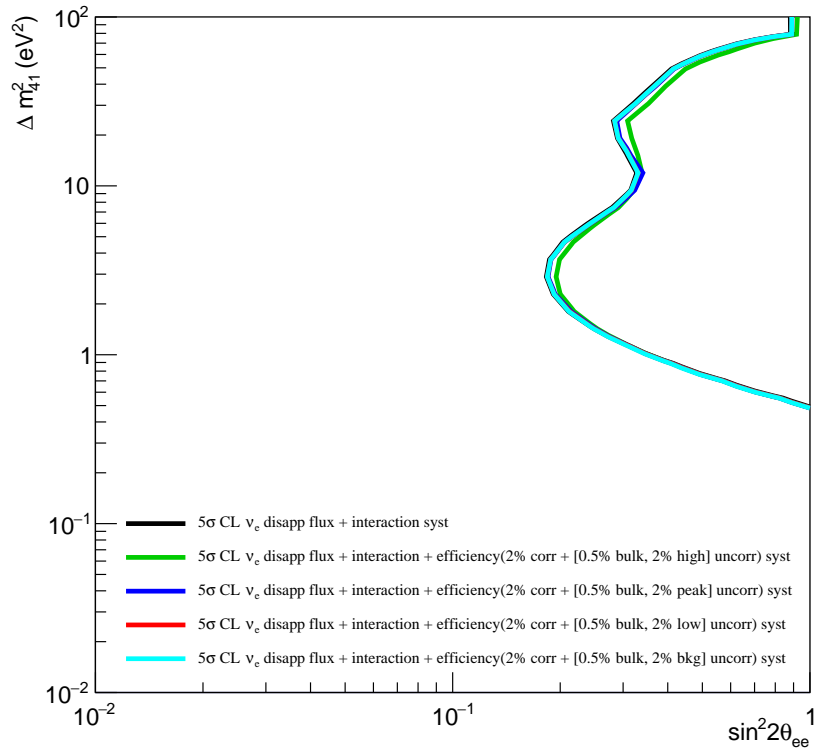


**Figure 1.36.:** The impact on the  $\nu_e$  disappearance exclusion sensitivity by applying a 2% fully correlated efficiency uncertainty for each of the SBN detectors and a 0.5% uncorrelated uncertainty for all but a single set of bins where the uncorrelated uncertainty is set to 2%. The 'peak' energy bins are defined as those covering an energy range of [0.6, 1.0] GeV. The 'high' and 'low' energy bins are defined as those covering energies above and below the peak energy respectively and the 'bkg' bins are all the bins associated with background events. The set of bins of interest are applied to each of the three detectors.

## Appendix A.

### Pointless extras

## Appendix B.

# Single Parameter Variations

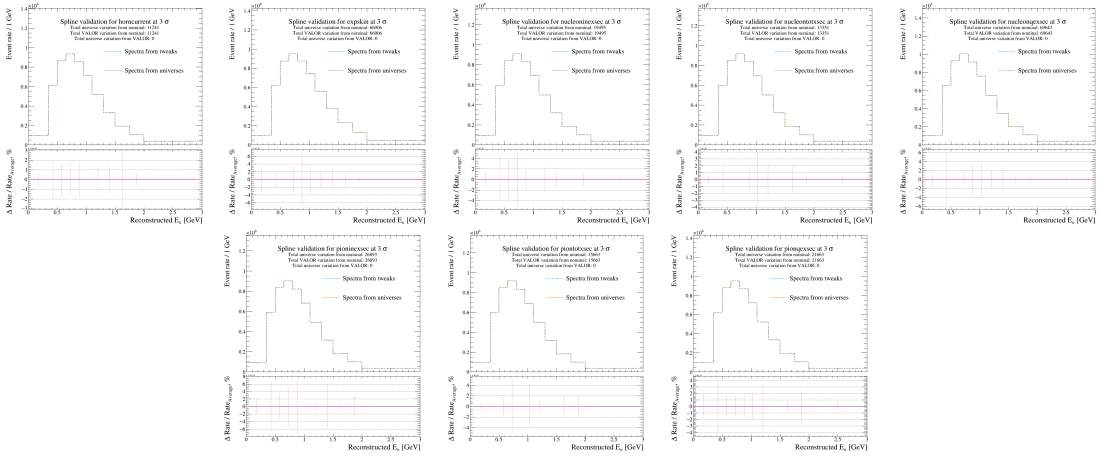


**Figure B.1.:** A comparison of the  $\pm 3\sigma$  variations from the response functions used by VALOR and the universes for the complete set of uncorrelated flux systematic parameters.

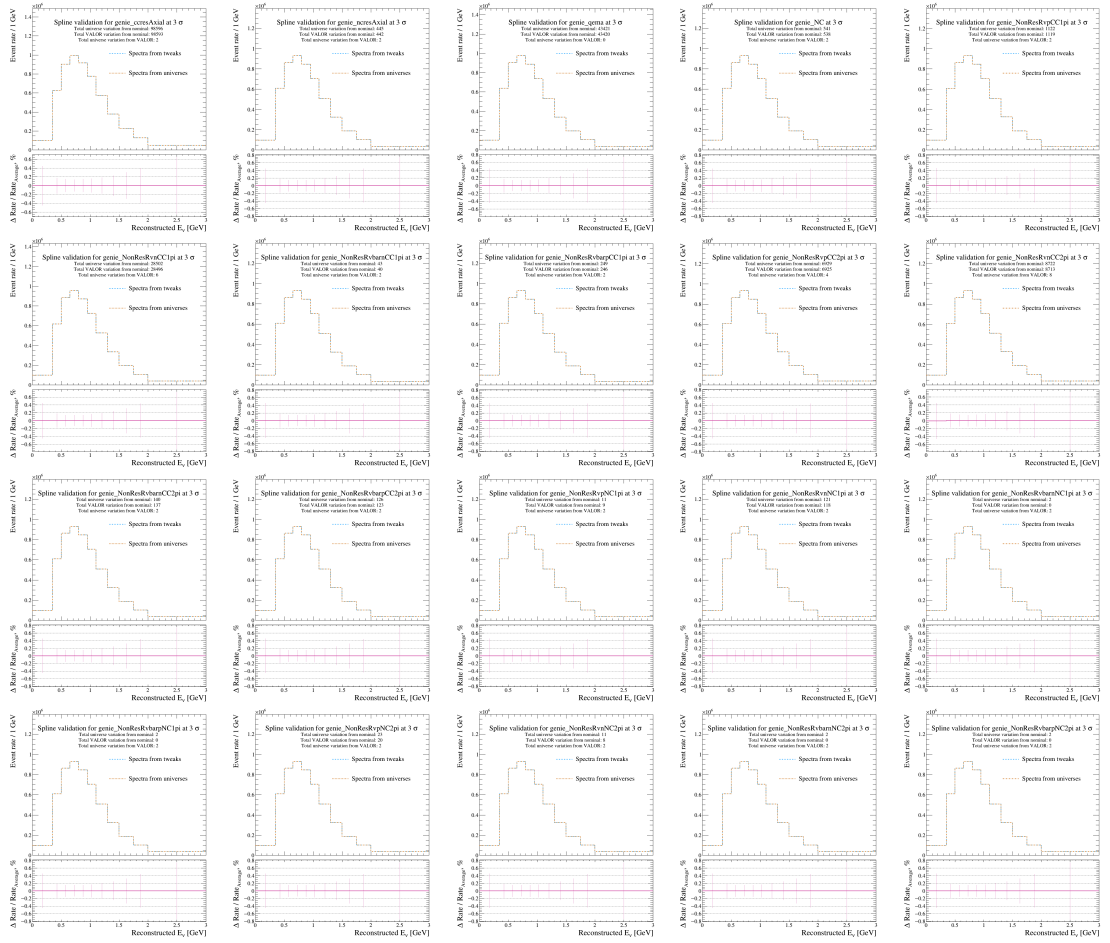


**Figure B.2.:** A comparison of the  $+3\sigma$  variations from the response functions used by VALOR and the universes for the complete set of proposal interaction systematic parameters.

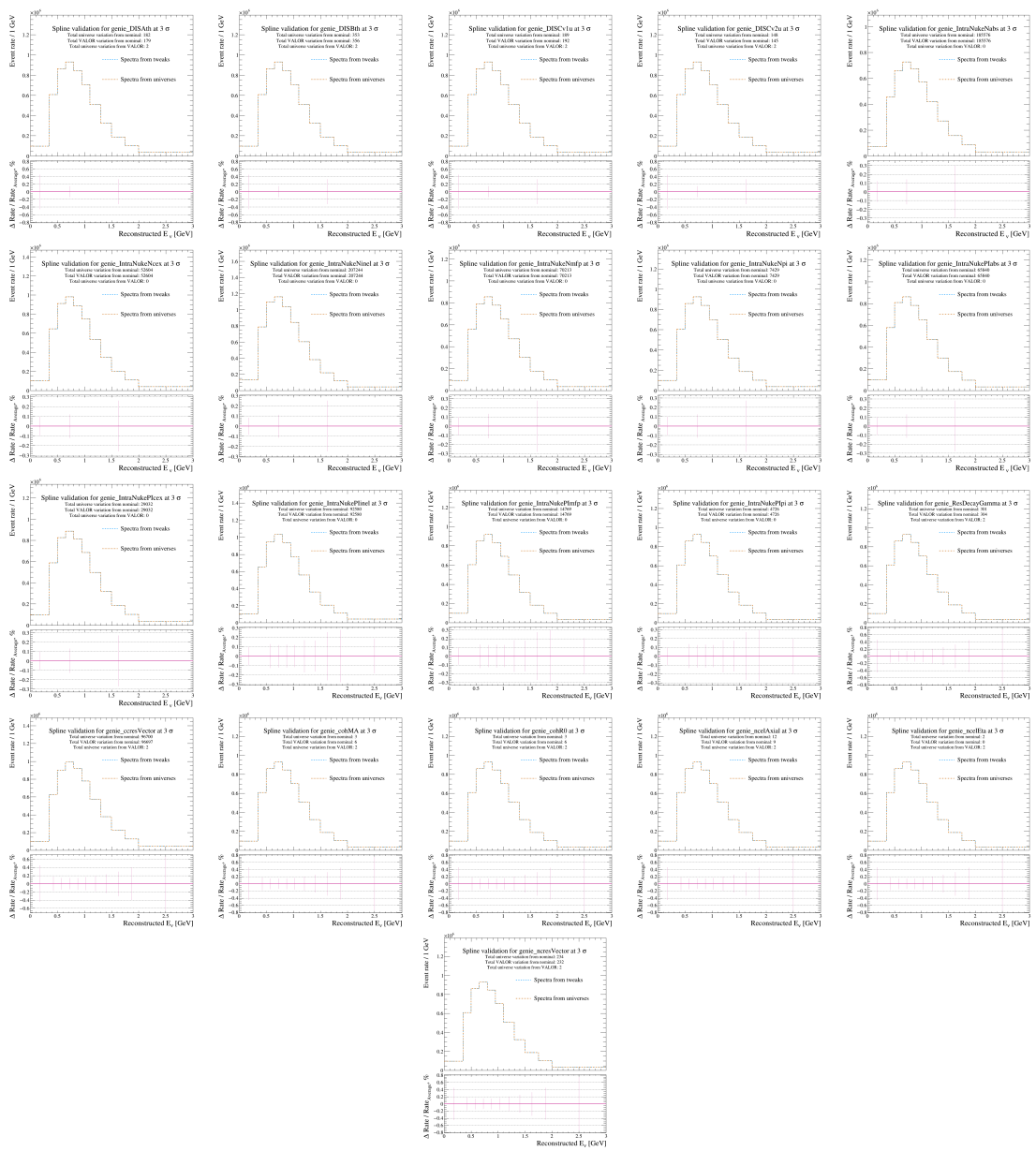


**Figure B.3.:** A comparison of the  $+3\sigma$  variations from the response functions used by VALOR and the universes for the complete set of modern cross-section systematic parameters.

## Appendix C.

### Detector Volumes

	X [cm]	Y [cm]	Z [cm]
Active Volume			
SBND	-199.15 – 199.15	-200.00 – 200.00	0.00 – 500.00
MicroBooNE	-1.55 – 254.80	-115.53 – 117.47	0.10 – 1036.90
ICARUS Module 1	-364.49 – -67.94	-173.41 – 143.41	-909.95 – 879.95
ICARUS Module 2	67.94 – 364.49	-173.41 – 143.41	-909.95 – 879.95
Fiducial Volume			
SBND TPC 1	-190.90 – 5.60	-185.00 – 185.00	15.00 – 415.00
SBND TPC 2	10.90 – 190.90	-185.00 – 185.00	15.00 – 415.00
MicroBooNE	-1.55 – 229.80	-90.53 – 92.47	30.10 – 986.90
ICARUS TPC 1	-339.49 – -221.04	-148.41 – 118.41	-879.95 – 829.95
ICARUS TPC 2	-218.89 – -92.94	-148.41 – 118.41	-879.95 – 829.95
ICARUS TPC 3	92.94 – 211.39	-148.41 – 118.41	-879.95 – 829.95
ICARUS TPC 4	214.39 – 339.39	-148.41 – 118.41	-879.95 – 829.95

**Table C.1.:** The dimensions defining the active and fiducial volumes for each SBN detector using their respective coordinate systems.

# Colophon

This thesis was made in L<sup>A</sup>T<sub>E</sub>X 2 <sub>$\varepsilon$</sub>  using the “hepthesis” class.

# Bibliography

- [1] C. Andreopoulos *et al.*, The VALOR Group, <https://valor.pp.rl.ac.uk>.
- [2] C. Andreopoulos *et al.*, VALOR DUNE Joint Oscillation and Systematics Constraint Fit (Version 2016a v2), [DUNE DocID 1291](#), 2016.
- [3] P. G. Hoel, *Introduction to Mathematical Statistics*, Fourth ed. (John Wiley & Sons, 1971).
- [4] A. G. Frodesen, O. Skjeggestad, H. Tøfte, *PROBABILITY AND STATISTICS IN PARTICLE PHYSICS* (Columbia University Press, 1979).
- [5] M. Dentler *et al.*, Updated global analysis of neutrino oscillations in the presence of eV-scale sterile neutrinos, [doi:10.1007/jhep08\(2018\)010](https://doi.org/10.1007/jhep08(2018)010), Journal of High Energy Physics **2018** (2018).
- [6] K. Abe *et al.*, The T2K experiment, [doi:<https://doi.org/10.1016/j.nima.2011.06.067>](https://doi.org/10.1016/j.nima.2011.06.067), Nuclear Instruments and Methods in Physics Research Section A: Accelerators, Spectrometers, Detectors and Associated Equipment **659**, 106 (2011).
- [7] K. Abe *et al.*, Search for short baseline  $\nu_e$  disappearance with the T2K near detector, [doi:10.1103/physrevd.91.051102](https://doi.org/10.1103/physrevd.91.051102), Physical Review D **91** (2015).
- [8] MINOS+, G. Tzanankos *et al.*, MINOS+: a Proposal to FNAL to run MINOS with the medium energy NuMI beam, [doi:10.2172/1028838](https://doi.org/10.2172/1028838), (2011).
- [9] K. B. M. Mahn *et al.*, Dual baseline search for muon neutrino disappearance at  $0.5\text{eV}^2 < \Delta m^2 < 40\text{eV}^2$ , [doi:10.1103/physrevd.85.032007](https://doi.org/10.1103/physrevd.85.032007), Physical Review D **85** (2012).

- [10] M. Aartsen *et al.*, Searching for eV-scale sterile neutrinos with eight years of atmospheric neutrinos at the IceCube Neutrino Telescope, [doi:10.1103/physrevd.102.052009](https://doi.org/10.1103/physrevd.102.052009), Physical Review D **102** (2020).
- [11] P. Adamson *et al.*, Search for Sterile Neutrinos in MINOS and MINOS+ Using a Two-Detector Fit, [doi:10.1103/physrevlett.122.091803](https://doi.org/10.1103/physrevlett.122.091803), Physical Review Letters **122** (2019).
- [12] R. Jones, *Muon-neutrino disappearance with multiple liquid argon time projection chambers in the Fermilab Booster neutrino beam*, PhD thesis, [doi:10.17638/03143192](https://doi.org/10.17638/03143192), University of Liverpool, 2021.